Inhibition of *Mycobacterium tuberculosis* DosRST two-component regulatory system signaling by targeting response regulator DNA binding and sensor kinase heme

Huiqing Zheng[1], Bilal Aleiwi[2], Edmund Ellsworth[2], and Robert B. Abramovitch[1*]

[1]Department of Microbiology and Molecular Genetics, [2]Department of Pharmacology and Toxicology, Michigan State University, East Lansing, Michigan, 48824

[‡]*Corresponding Author*

Robert B. Abramovitch

E-mail: abramov5@msu.edu

Phone: (517) 884-5416

Fax: (517) 353-8957

Abstract

Mycobacterium tuberculosis (Mtb) possesses a two-component regulatory system, DosRST, that enables Mtb to sense host immune cues and establish a state of non-replicating persistence (NRP). NRP bacteria are tolerant to several anti-mycobacterial drugs and are thought to play a role in the long course of tuberculosis (TB) therapy. Therefore, small molecules that inhibit Mtb from establishing or maintaining NRP could reduce the reservoir of drug tolerant bacteria and function as an adjunct therapy to reduce treatment time. Previously, we reported the discovery of six novel chemical inhibitors of DosRST, named HC101A-106A, from a whole cell, reporter-based phenotypic high throughput screen. Here, we report functional and mechanism of action studies of HC104A and HC106A. RNAseq transcriptional profiling shows that the compounds downregulate genes of the DosRST regulon. Both compounds reduce hypoxia-induced triacylglycerol synthesis by ~50%. HC106A inhibits Mtb survival during hypoxia-induced NRP, however, HC104A did not inhibit survival during NRP. An electrophoretic mobility assay shows that HC104A inhibits DosR DNA binding in a dose-dependent manner, indicating that HC104A may function by directly targeting DosR. In contrast, UV-visible spectroscopy studies suggest HC106A directly targets the histidine kinase heme, via a mechanism that is distinct from the oxidation and alkylation of heme previously observed with artemisinin (HC101A). Synergistic interactions were observed when DosRST inhibitors were examined in pair-wise combinations with the strongest potentiation observed between artemisinin paired with HC102A, HC103A, or HC106A. Our data collectively show that the DosRST pathway can be inhibited by multiple distinct mechanisms.

Keywords: Chemical biology, two-component regulatory systems, microbial pathogenesis.

50 **Introduction**

51 *Mycobacterium tuberculosis* (Mtb) is the causative agent of tuberculosis (TB). Mtb is an
52 intracellular pathogen that can latently infect the host without causing disease symptoms (1).
53 During chronic infection, it can establish a dormant state known as non-replicating persistence
54 (NRP) where Mtb modulates its metabolism in response to environmental and host immune cues,
55 such as hypoxia, acidic pH, and nutrient starvation (2, 3). DosRST is a two-component regulatory
56 system that regulates Mtb persistence (4-6). It consists of two sensor histidine kinases, DosS and
57 DosT, and the cognate response regulator DosR, which regulates expression of about 50 genes
58 in the DosRST regulon (6-8). The pathway can be induced by host intracellular stimuli, such as
59 nitric oxide (NO), carbon monoxide (CO) and hypoxia, through DosS and DosT (9-11). DosS is
60 an oxygen and redox sensor, whereas DosT acts an oxygen sensor (12-14). Both kinases sense
61 ligands via the heme group, and are inactive when the heme exists as either the Met (Fe^{3+}) form
62 (DosS) or the oxy (Fe^{2+}-O_2) form (DosT) in the presence of O_2 (13). However, hypoxic conditions
63 activate the kinases by inducing the conversion of DosS to the ferrous form and DosT to the deoxy
64 form. Therefore, DosS/T play overlapping and distinct roles in sensing the redox status and
65 oxygen level of the environment to turn on the DosR pathway (11, 15).

66 Non-replicating bacilli are naturally tolerant to many anti-mycobacterial drugs, such as
67 isoniazid (INH) that only kills replicating Mtb (16-18). During TB infection, the disease presents
68 as a spectrum of replicating and non-replicating bacteria; the NRP population of bacteria are
69 thought to be responsible, in part, for the 6-month long course of TB treatment. This long antibiotic
70 regimen makes controlling the TB epidemic challenging and has likely contributed to the evolution
71 of drug-resistant Mtb strains. Therefore, there exists an urgent need to identify new strategies to
72 treat the disease, with a particular focus on discovering new ways to shorten the course of TB
73 therapy. Targeting the DosRST pathway is a promising strategy, because *dosRST* mutants are
74 attenuated in *in vitro* models of hypoxia-driven NRP (19) and in animal models that generate
75 hypoxic granulomas, including non-human primates, guinea pigs, and C3HeB/FeJ mouse models

76 of TB infection (4, 20-22). Furthermore, deletion of DosR-regulated gene *tgs1*, which is involved
77 in triacylglycerol (TAG) synthesis, causes reduced antibiotic tolerance (23, 24). Therefore,
78 inhibiting the DosRST pathway and killing the reservoir of NRP bacteria may function to narrow
79 the spectrum of TB disease and shorten the course of TB therapy.

80 Fluorescent reporter strains can be used as tools in drug discovery to conduct targeted,
81 whole cell phenotypic screens for pathways that play a role during pathogenesis, but have limited
82 impact when bacteria are grown *in vitro*(25, 26). In an effort to discover the new chemical probes
83 that inhibit Mtb persistence, we previously performed a whole cell phenotypic high throughput
84 screening (HTS) of a >540,000 compound library using the DosRST regulon reporter strain
85 CDC1551 (*hspX'::*GFP) (27). We discovered six compounds that inhibit the DosR-dependent,
86 hypoxia-induced GFP fluorescence. In the previous report, we showed that the HC101, HC102
87 and HC103 series functioned to inhibit NRP associated physiologies, including TAG accumulation,
88 survival during hypoxia and isoniazid tolerance. Mechanism of action studies showed that the
89 HC101 series, composed of artemisinin and related analogs, functioned by oxidizing and
90 alkylating the DosS and DosT heme. HC102 and HC103 did not modulate the DosS/T heme, and
91 were instead found to inhibit sensor kinase autophosphorylation. Here, we report the
92 characterization of two additional compounds, HC104A and HC106A. Transcriptional and
93 biochemical analysis demonstrate that both compounds function to downregulate the DosRST
94 pathway and inhibit persistence associated physiologies. Biochemical studies show HC104A and
95 HC106A function by distinct mechanisms of action, with HC104A inhibiting DosR DNA binding
96 and HC106A interacting with DosS and DosT heme to block environmental sensing. Studies
97 examining the pair-wise interactions between the five DosRST inhibitors revealed synergistic
98 interactions, including strong potentiating interactions of artermisinin and HC106A. Structure
99 activity relationship studies of HC106 identified functional groups of HC106A that are required for
100 activity and enabled optimization of HC106 potency to nanomolar effective concentrations against
101 whole cell Mtb.

102 **Results**

103 ***Inhibition of the DosR regulon by HC104A and HC106A***

104 Characterization studies were undertaken with two putative DosRST regulon inhibitors,
105 HC104A and HC106A (Fig. 1a) (27). Half-maximal effective concentration (EC_{50}) studies using
106 the CDC1551 (*hspX'::GFP*) DosRST-dependent fluorescent reporter strain, show that HC104A
107 and HC106A inhibit DosRST-dependent GFP florescence with EC_{50} values of 9.8 μM and 2.48
108 μM, respectively (Fig. 1b and 1c).

109 The compounds have minimal impact on Mtb growth, suggesting they are also potential
110 DosRST inhibitors, as DosRST is not required for survival under the conditions of mild hypoxia
111 used in the reporter-based assay. RNA-seq-based transcriptional profiling was undertaken to
112 determine if the DosRST regulon was inhibited by the compounds. Mtb was treated with 40 μM
113 HC104A, HC106A or dimethyl sulfoxide (DMSO) control for 6 d in a standing flask, and following
114 incubation RNA was extracted, sequenced and analyzed for differential gene expression relative
115 to the DMSO control. As a control for the DosR regulon, transcriptional profiling was also
116 previously conducted on a DMSO treated CDC1551(Δ*dosR*) mutant strain (27). The
117 transcriptional profiles showed that the genes strongly repressed by HC104A and HC106A (>2-
118 fold; $q<0.05$) are from the *dosR* regulon (Fig. 2a-c, Supplementary Dataset 1, 3).

119 HC106A exhibited a remarkably strong reduction of gene expression, with transcripts for
120 *tgs1* and *hspX* being almost undetectable by RNA-seq following HC106A treatment. Interestingly,
121 while HC106A broadly inhibited genes of the DosRST regulon, HC104A only strongly inhibited
122 part of the DosR regulon, with the strongest inhibition reserved for *hspX*, the promoter used to
123 drive reporter fluorescence in the screen. These RNA-seq results were validated by semi-
124 quantitative RT-PCR, with HC104A causing downregulation of *dosR*, *hspX*, and *tgs1 in vitro* by
125 6-, 570- and 13-fold, respectively; whereas HC106A downregulated these three genes by 49-,

126 1360-, and 1424-fold, respectively (Supplementary Fig. 1), with *hspX* and *tgs1* transcripts being
127 below the level of detection by qRT-PCR.

128 Comparisons of transcriptional profiles from the inhibitor treated wild type (WT) Mtb strain
129 to a CDC1551(Δ*dosR*) mutant strain showed that there are a total of 26 genes and 53 genes from
130 *dosR* regulon inhibited by HC104A and HC106A, respectively. Notably, HC104A and HC106A
131 caused an additional 119 genes and 35 genes to be repressed that were not repressed in the
132 CDC1551(Δ*dosR*) mutant strain (Fig. 2c). This observation suggested that these two compounds
133 exhibit some DosR-independent activities. To confirm the specificity of the compounds, RNA-seq
134 was also performed on CDC1551(Δ*dosR*) mutant background (Supplementary Dataset 2-3)
135 treated with HC104A or HC106A. This analysis identified 171 genes and 51 genes that are
136 downregulated (>2-fold; $q<0.05$) by HC104A and HC106A, respectively (Fig. 2d). This finding
137 indicates that HC104A and HC106A impact other targets beside DosR regulon, with HC106A
138 showing greater on-target specificity than HC104A. Based on these findings, we conclude that:
139 1) HC106A strongly and specifically inhibits the DosRST regulon; and 2) HC104A strongly inhibits
140 a portion of the DosRST regulon, with several notable off-target activities.

141 To assess the impact of the inhibitors on the DosRST pathway on intracellular Mtb, murine
142 bone marrow-derived mouse macrophages were infected with Mtb and treated with 40 μM
143 HC104A and HC106A for 48 h. Total bacterial RNA was isolated and analyzed by RT-PCR for
144 *hspX* and *tgs1* gene differential expression. The results demonstrate that the induction of *hspX*
145 and *tgs1* were inhibited 185- and 10-fold by HC104A and 6- and 4-fold by HC106A, respectively
146 (Fig. 3a). These finding confirm that HC104A and HC106A can access Mtb inside the
147 macrophage, however, the reduced repression of the pathway by HC106A as compared to broth
148 culture, suggests that the molecule may not be able to efficiently target intracellular Mtb.

149 The DosRST pathway is also induced by redox signals such as vitamin C and NO (27).
150 To examine whether HC104A and HC106A can repress the induction of DosRST pathway by

151 vitamin C or NO, Mtb cells were pretreated with HC104A or HC106A for 24 h followed by vitamin
152 C or NO induction for 2 h. The expression of DosR-regulated genes (*hspX* and *tgs1*) was
153 examined by real time-PCR. Vitamin C and DETA-NONOate (NO donor) strongly induced *hspX*
154 and *tgs1* as previously reported ((27), Fig. 3b). For instance, vitamin C induced *hspX* and *tgs1* by
155 2162- and 58-fold, respectively; whereas DETA-NONOate upregulated *hspX* and *tgs1* 3024- and
156 113-fold, respectively (Fig. 3b). Mtb cells pretreated with HC106A showed strong inhibition of
157 *hspX* and *tgs1* induction by vitamin C and DETA-NONOate. For example, HC106A inhibited the
158 *hspX* and *tgs1* transcripts by 78- and 14-fold following vitamin C treatment, respectively, and 362-
159 and 151-fold following DETA-NONOate treatment. Following vitamin C treatment, HC104 showed
160 inhibition of *hspX* by 3.4-fold and no effect on *tgs1*, or 302- and 6.6-fold inhibition of *hspX* and
161 *tgs1* following DETA-NONOate treatment. These findings show that HC104A and HC106A act as
162 inhibitors of the DosRST pathway in response to redox signals in addition to hypoxia.
163
164 ***Inhibition of Mtb persistence-associated physiologies***
165 Mtb accumulates TAG during hypoxia (27-29). DosR directly regulates *tgs1*, which
166 encodes a TAG synthase that is involved in the last step of TAG biosynthesis and is required for
167 TAG accumulation during hypoxia (30). Transcriptional profiling showed that HC104A and
168 HC106A repress expression of *tgs1*. Based on this transcriptional profiling, we hypothesized
169 these two compounds may inhibit TAG biosynthesis during NRP. To test our hypothesis, Mtb cells
170 were radiolabeled with ^{14}C-acetate and treated with HC104A or HC106A for 6 d. Lipids were
171 isolated and analyzed by thin layer chromatography (TLC). As previously observed, DMSO
172 treated CDC1551(Δ*dosR*) mutant displayed a strong (87%) reduction of TAG accumulation as
173 compared to DMSO treated WT (Fig. 3c and Supplementary Fig. 2). Mtb cells treated with
174 HC104A or HC106A showed a ~50% reduction of TAG accumulation, supporting our hypothesis
175 that the compounds can inhibit TAG biosynthesis.

176 DosRST has been previously reported to be required for survival during NRP, where
177 deletion of DosR causes greatly reduced survival during prolonged hypoxic stress (19). The
178 impact of HC104A and HC106A on Mtb survival during NRP was examined using the hypoxic
179 shift-down model (27). Mtb survival was examined following 10 d of treatment with the compounds
180 at 40 μM. The Δ*dosR* mutant control had 15% survival relative to DMSO, and was partially
181 complemented, supporting the proposal that survival during hypoxia is DosR dependent. Mtb cells
182 treated with HC106A displayed 50% survival relative to DMSO control (Fig. 3d), whereas,
183 HC104A had no impact on Mtb survival during NRP, an observation that suggests the portion of
184 the DosR regulon inhibited by HC104A is not essential for survival during NRP.
185
186 ***HC104A inhibits DosR DNA binding***
187 There are several potential targets of HC104A and HC106A to directly inhibit DosRST
188 signaling, including: 1) direct inhibition of DosS/T sensor kinase activity, 2) modulation of the
189 heme in the sensor, or 3) inhibition of DosR binding of DNA. To investigate the biochemical
190 mechanisms of action of HC104A and HC106A, inhibition of DosS autophosphorylation was
191 initially evaluated. The DosS protein was treated with different concentrations of HC104A and
192 HC106A from 10 μM to 40 μM, or with 40 μM HC103A as a positive control that was previously
193 discovered to be a DosS/T autophosphorylation inhibitor (27). As previously observed, HC103A
194 strongly inhibited DosS autophosphorylation, but HC104A and HC106A had no inhibitory activity
195 (Supplementary Fig. 3). This suggests HC104A and HC106A are not directly inhibiting DosS/T
196 autophosphorylation activity.
197 Next, a UV-visible spectroscopy assay was employed to investigate if HC104A targets to
198 the heme of the sensor kinase DosS. Treatment of DosS protein with the reducing agent dithionite
199 (DTN) caused a shift of the Soret peak from 403 nm to 430 nm as previously described (13, 27).
200 Addition of HC104A to reduced DosS did not shift the peak to the oxidized position, suggesting

201 that HC104A does no modulate DosS heme redox (Supplementary Fig. 4). Together, these data
202 indicate that HC104A does not inhibit DosRST signaling by targeting sensor kinase
203 autophosphoryation or heme and supported examining DosR as a potential target.

204 Inspection of the HC104A structure revealed it had significant similarity to the compound
205 virstatin (31). Virstatin is an anti-virulence compound that inhibits *Vibrio cholera* cholera toxin
206 production by targeting the transcription regulator ToxT (31). Virstatin inhibits ToxT protein
207 dimerization and subsequently interferes with DNA binding, thereby inhibiting the transcription of
208 downstream genes involved in toxin production. Based on the similarity of chemical structure
209 between HC104A and virstatin, we hypothesized that HC104A may be targeting DosR, and
210 interfering with DNA binding. To test this hypothesis, an electrophoretic mobility shift assay
211 (EMSA) was employed to investigate the impact of HC104A on DosR DNA binding. Recombinant
212 DosR protein, ranging from 0.5 μM to 4 μM, was treated with 40 μM HC104A or a DMSO control
213 and tested for binding to fluorescently labeled *hspX* promoter DNA. In the DMSO treated control,
214 DosR bound promoter DNA beginning at a concentration 2 μM DosR protein (Fig. 4a). Treating
215 the reaction containing 2 μM DosR protein with HC104A significantly inhibited DNA binding by
216 ~22-fold compared to DMSO control (Fig. 4b). To further characterize the impact of HC104A on
217 DosR binding of DNA, a dose-response study was performed. Reactions containing 2 μM
218 recombinant DosR proteins were treated with different concentrations of HC104A or virstatin
219 ranging from 1 – 80 μM. HC104A inhibited DosR binding of DNA beginning at 10 μM HC104A.
220 The fraction of free DNA increased as HC104A concentration increased (Fig. 3.4c). For example,
221 the fraction of free DNA was 72%, 89%, 92%, 96% and 100% for 20 μM, 30 μM, 40 μM, 60 μM
222 and 80 μM HC104A, respectively, whereas DMSO control had 15% free DNA (Fig. 4d). Thus,
223 HC104A significantly inhibits DosR-DNA binding in a dose-dependent manner. Reactions treated
224 with virstatin had no impact on DosR binding of DNA (Supplementary Fig. 5a). Consistent with
225 these observations, virstatin did not have any impact on DosRST signaling in the whole cell Mtb

226 fluorescence reporter assay (Supplementary Fig. 5b). These findings support the hypothesis that
227 HC104A may function by inhibiting DosR DNA binding activity and has an activity that is distinct
228 from the related molecule virstatin.
229
230 ***HC106A modulates DosS heme***
231 DosS and DosT have a channel that exposes the heme to the environment and enables
232 interactions with gases (32, 33). This channel is an Archilles heel that can be targeted by small
233 molecules. Previously, it was shown that the artemisinin modulates DosS/T by oxidizing and
234 alkylating heme carried by the kinases (27). UV-visible spectroscopy studies were conducted to
235 examine if HC106A modulated DosS heme. Recombinant DosS was purified from *E. coli*,
236 degassed and the change of DosS heme spectrum was monitored under anaerobic conditions by
237 UV-visible spectroscopy. Treating DosS with the reducing agent dithionite (DTN) caused the Soret
238 peak to shift to 430 nm as shown previously (13, 27). HC106A was added to the reaction following
239 DTN treatment to observe the impact on the DosS heme UV-visible spectrum. HC106A caused
240 the DosS Soret peak to immediately shift to 422 nm, where the peak was stably maintained for 2
241 h (Fig. 5a). This spectrum shift is different from artemisinin, where under identical conditions,
242 artemisinin causes the DosS Soret peak to gradually shift back to the oxidized state at 403 nm
243 (27). These findings show that HC106A may also interact with sensor kinase heme, but via a
244 mechanism that is distinct from artemisinin-heme interactions.
245 The Soret peak at 422 nm is consistent with previously described spectra that are
246 observed when DosS heme interacts with NO or CO (13). To confirm this observation, DosS was
247 treated with 100 μM CORM-2 (a CO donor) which caused a shift of the Soret peak to 422 nm,
248 similar to what was observed for HC106A (Fig. 5b). This finding supports a hypothesis that
249 HC106A may also be directly binding to the heme. Notably, CO activates DosS kinase function,
250 whereas HC106A functions to inactivate the regulon, demonstrating that the impact of heme
251 binding by CO or HC106A has differing impacts on the sensor kinase switch.

252 Amino acid substitutions in the channel exposing the DosS heme to the environment, such
253 as DosS E87L or G117L, can limit access of artemisinin to modulate heme (27). To support the
254 hypothesis that HC106A directly targets DosS heme, we tested the impact of these amino acid
255 substitutions on HC106A/DosS heme interactions. Treating DosS(E87L) with HC106A exhibited
256 a profile similar to wild type DosS with the Soret peak shifting to 422 nm (Supplementary Fig. 6).
257 However, DosS(G117L) had no change to the overall spectrum after HC106A treatment (Fig.
258 3.5c). This finding indicates that DosS(G117L) is resistant to HC106A, and confirms that HC106A
259 accesses the heme via a similar mechanism as artemisinin.
260 To confirm DosS is a target of HC106A in Mtb, we examined the impact of overexpressing
261 DosS protein in Mtb. If DosS is the target of HC106A, overexpression may reduce the
262 effectiveness of HC106A. WT DosS protein was constitutively expressed from the *hsp60* promoter
263 in Mtb. The vector control showed that both *hspX* and *tgs1* genes were downregulated by HC106A
264 by 2331- and 3470-fold, respectively (Fig. 5d). Overexpressing DosS provided significant
265 resistance to HC106A, with *hspX* and *tgs1* showing 23- and 16.5-fold less inhibition, respectively,
266 relative to the empty vector control This observation of resistance in Mtb is consistent with the
267 biochemical data supporting the view that DosS is a direct target of HC106A.
268
269 ***Synergistic interactions between DosRST inhibitors***
270 With multiple distinct inhibitory activities of the HC101A, HC102A, HC103A, HC104A and
271 HC106A, we sought to examine if potentiating or antagonistic interactions existed between the
272 molecules, when targeting the DosRST pathway. To examine these interactions, checkboard
273 assays were performed with pairwise comparisons of artemisinin (HC101A), HC102A, HC103A,
274 HC104A and HC106A. CDC1551 (*hspX'::*GFP) was treated with combinations of two compounds
275 ranging from 50 μM to 0.08 μM in 96-well plates. DosR-driven GFP fluorescence and optical
276 density were measured following 6 d of treatment. The Combination Index (CI) was calculated for
277 each drug pair based on the Chou-Talalay method in the CompuSyn software package (34, 35),

278 where CI values of < 1, = 1 and >1 indicate synergistic, additive or antagonistic interactions,
279 respectively. Among all 64 compound pairs, artemisinin combined with HC102A, HC103A,
280 HC104A and HC106, showed 46, 49, 41, and 50 combinations that have CI <1, respectively (Fig.
281 3.6). Notably, some CI values are below 0.1 when artemisinin was paired with HC102A, HC103A
282 or HC106A combinations. Example dose response curves illustrate these synergistic interactions
283 (Fig. 6). Several other pairwise comparisons also demonstrated synergy (Supplementary Fig. 7),
284 however, in general, these interactions had CI between 1 and 0.1, supporting weaker synergistic
285 interactions, as compared to combinations with artemisinin. Overall, these studies provide the
286 evidence that the inhibitors function by distinct mechanisms and may be combined to improve
287 potency.
288
289 ***Structure-activity relationship study for HC104A and HC106***
290 We conducted a catalog search for HC104 and HC106 analogs and obtained 10
291 commercial analogs for each series to define initial structure activity relationships (SAR). For
292 HC104A we observed that a bromine in the 5-position is required for activity and that the R2
293 dimethylamine group is not required (Supplementary Table 1). For example, HC104B is identical
294 to HC104A except for the removal of the bromine (R1), which results in a complete loss of activity
295 in the whole cell assay. Whereas, replacement of the R2 group with a methyl (HC104G) results
296 in an active compound, although ~5-fold less active than HC104A. Although not highly potent, its
297 ligand efficiency, cLogD and druglikeness are in the range of what would be considered
298 acceptable to good as a starting point for further manipulation. For HC106A (Table 1), catalog
299 SAR work led to new understandings of the nature of the series. We first found that the simple
300 removal of an ortho chloro on the "A" ring of HC106A leads to ~ 2-fold enhanced activity, with an
301 EC_{50} in the whole cell Mtb assay for DosRST inhibition of 1.33 μM (HC106F). It was also found
302 that the use of an alternative isomer of the isoxazole had no detectable activity (HC106C).
303

304 To further understand the SAR of the HC106 series, additional analogs were
305 synthesized to examine the need of the central urea functionality and whether modifications can
306 be tolerated (Table 1). A pyridyl analog (MSU-41425), designed to replace the isoxazole also
307 demonstrated no activity as was the symmetrical 4-chloroaniline derived urea (MSU-41324).
308 However, the bis-isoxazole urea (MSU-39444) provides an EC_{50} of 1.7 μM, indicating that the
309 isoxazole is important for function. Isoxazoles are unique among heterocycles in that they exist
310 in multiple tautomeric forms as supported by initial NMR studies (36). We next explored the
311 need of one of the -NHs of the urea, capping it with a methyl (MSU-39451), integrating it into a
312 ring for conformational restriction (MSU-39453), and replacing with a methylene unit (MSU-
313 39449). In all cases, reduced activity (0.5 - 1 log) was observed but not all activity was lost.
314 Thus, HC106A is a potent whole cell inhibitor of the DosRST pathway, with flexibility to be
315 improved via SAR.

316 To further test the SAR, we conducted a Topliss Tree evaluation of the "A-ring" aniline
317 (Table 20)(37). To reliably prepare the derivatives, we explored and established a general
318 preparation (Supplementary Fig. 8). This route is preferred relative to alternative approaches
319 for its cleanliness, yields and ease of purification, usually by trituration. It is also anticipated
320 that it will allow access to future derivatives. Using HC106F and HC106A as starting points, we
321 prepared the 3,4-diclorochloro and 3-chloro derivatives (MSU-39452 and MSU-39445,
322 respectively). Both the 3- and 4-chloro derivatives demonstrated greater activity than 3,4-
323 dichloro (MSU-39452). We found that replacing the 4-chlorophenyl ring with pyridyl analogs
324 (MSU-39448 and MSU-39450) lead to similar activity. Focusing on 4-position derivatives, we
325 found that fluoro (MSU-39446), bromo (MSU-41464) and methoxy (MSU-39447), as electron p-
326 orbital donating substituents, also lead towards incrementally increased activity. Para-t-butyl
327 phenyl (MSU-41442), provided slightly diminished activity. Electron withdrawing substituents,
328 such as 4-CO_2Me (MSU-4165), 4-trifluoromethyl (MSU-41463) and biphenyl (MSU-41443) saw
329 activity similar to the 4-chlorophenyl derivative (HC106F). Overall, several analogs were

330 discovered with significantly ~4-fold enhanced potency, with several inhibitors having whole cell
331 DosRST inhibitory EC_{50} below 1 μM, including EC_{50} of 0.63 μM, 0.61 μM, 0.54 μM and 0.75 μM
332 for MSU-33189, -39447, -39446, and -39455, respectively. The parent analog HC106A had an
333 EC_{50} of 2.48 μM.

334 There appears to be little sensitivity, positive or negative, for electron-drawing
335 substituents other than the biphenyl derivative (MSU-41443), which is likely the result of
336 negative steric interactions in the binding domain. Additional derivatives (replacement of
337 dichlorophenyl) were also prepared to further probe the size and nature of the binding domain.
338 We began by replacing the chlorophenyl ring of HC106F with benzyl- (MSU-41462), isobutyl-
339 (MSU-41542), cyclopentyl- (MSU-41546) and cyclohexyl- (MSU-42002) analogs. All analogs
340 demonstrated similar activities, relative to HC106F and the simple phenyl analog (MSU-33189),
341 suggesting flexibility of fragments that could bind in this domain.

342 Kinetic solubility assays were conducted for selected analogs and all exhibited excellent
343 aqueous solubility greater than >100 μM, except for MSU-41443 (Table 2). This finding shows
344 that the urea group present in the HC106A does not have a detrimental impact on HC106
345 aqueous solubility. All of the tested deriviatives also demonstrated favorable mouse microsomal
346 stability, including. Overall, the nanomolar whole cell potency, flexible SAR, good microsomal
347 stability and excellent solubility, confirm that the HC106 series is a suitable series for continued
348 optimization to identify a drug-like lead.

349 DosRST is a two-component regulatory system required for Mtb environmental sensing,
350 adaptation, and persistence. By using a fluorescent reporter strain CDC1551 (*hspX'::GFP*), we
351 have previously discovered small molecule inhibitors of DosRST, named HC101A-HC106A, from
352 the whole-cell phenotypic HTS. Here, we report the characterizations of HC104A and HC106A as
353 DosRST inhibitors. Both compounds downregulated genes in the DosR regulon, and inhibited
354 TAG biosynthesis. HC106A also reduced Mtb survival during NRP.

355 In a UV-visible spectroscopy assay, we observed that HC106A interacts with the heme of
356 sensor kinase DosS. The UV-visible spectrum of HC106A-treated DosS is similar to those of CO-
357 or NO-treated DosS. The overlap between the CO and HC106A spectra supports that HC106A
358 may also directly bind to the heme of DosS. Interestingly, CO activates sensor kinases, whereas
359 HC106A inhibits them. This could be due to the difference in conformational changes induced by
360 CO and HC106A, or binding of HC106A may lock the sensor kinases into an inactive state.
361 Furthermore, the DosS G117L substitution in recombinant DosS blocks the heme exposing
362 channel and provides resistance to HC106A. This means that, similar to artemisinin, this channel
363 is also important for the activity of HC106A. These findings provide additional evidence that the
364 heme-exposing channel in DosS/T can be exploited by small molecules to inhibit the heme from
365 sensing signals and to disrupt signal transduction of a two-component regulatory system. To our
366 knowledge, these two distinct mechanisms of actions are novel mechanisms to inhibit the
367 DosRST pathway.

368 Mechanistic studies via EMSA indicates that HC104A may function by targeting DosR and
369 inhibiting DosR DNA binding. Virstatin had no effect on DosR DNA binding and no impact on the
370 DosRST signaling in whole cells, showing that although both compounds share a similar structure,
371 they function by distinct mechanisms. From the catalog SAR study, we found that the bromine
372 group is required for the compound. Virstatin does not have the bromine, and the R-group is
373 butyric acid instead of dimethylamine. These two differences are enough to differentiate the
374 activity of the compounds. Moreover, transcriptional profiling shows that the most repressed
375 genes by HC104A are from the DosR regulon, providing additional evidence that HC104A is
376 somewhat selective for specific DosR regulated genes. Interestingly, the genes most
377 downregulated by HC104A, including *hspX*, *Rv2030c*, *pfkB*, and *Rv2028c*, are from the same
378 operon under control of *hspX* promoter, which is strongly induced by DosR in hypoxia. This result
379 suggests that HC104A is more specific to target *hspX* operon genes as compared to other DosR
380 regulated genes. This finding leads to the speculation that HC104A may be more efficient to

381 prevent DosR binding to the *hspX* promoter than the other DosR promoters. HC104A may fit
382 better in the pocket in the interface of DosR-*hspX'* complex. This postulation also supports the
383 idea that HC104A may not have an impact on DosR protein dimerization, which would lead to
384 universal downregulation of DosR-regulated genes. Detailed characterizations of HC104A on
385 inhibiting DosR dimerization and promoter binding specificity is the subject of ongoing
386 characterizations.

387 This study together with the previous report reveals multiple distinct inhibitory mechanisms
388 for the five compounds, HC101A-104A, HC106A. Four out five compounds, HC101A-HC103A
389 and HC106A, are proposed to function by targeting the sensor kinases DosRST. Furthermore,
390 these four compounds are effective at decreasing Mtb survival during NRP in hypoxic-shift down
391 assay. In contrast, the compound targeting DosR, HC104A, had no impact on Mtb survival during
392 NRP. This result is consistent with a previous report that showed only the Δ*dosS* mutant exhibits
393 a survival defect in the C3HeB/FeJ mouse model (22). Notably, the *dosR* mutant strain used in
394 our study is also lacking *dosS* expression due to polar impacts of the deletion, supporting the
395 hypothesis that the reduced survival during NRP may be dependent on DosS. Alternatively, we
396 noted that HC104A only inhibits a portion of the DosR regulon with only 26 genes being
397 downregulated. This finding suggests that the DosR regulated genes that are inhibited by HC104A
398 (Fig. 2, and Supplementary Dataset 1, 3) are not required for DosRST-dependent persistence
399 during NRP or not sufficiently inhibited to have an impact on survival.

400 The transcriptional profiling data showed off-target impacts in the treated *dosR* mutant
401 strain. These effects may be due to inhibition of DosS/T signaling that functions independent of
402 the response regulator. Several recent studies have demonstrated the occurrence of cross-
403 interactions between histidine kinases and response regulators in Mtb. For instance, Lee *et al.*
404 shows that DosT can interact with the other non-cognate response regulators, including NarL and
405 PrrA (38). Our transcriptional profiling of the compound treated *dosR* mutant strain suggests that
406 some genes downregulated by HC101A, HC103A and HC106A may be DosS-dependent but

407 DosR-independent (Supplementary Fig 9). In the prior study, six genes are similarly regulated
408 between artemisinin and HC103A in the treated *dosR* mutant strain, including Rv0260c that
409 encodes a putative response regulator (27). HC106A and HC103A share four differentially
410 regulated genes in the *dosR* mutant, including *argC*, *argJ*, *argB*, and *argF*, which are genes
411 involved in arginine biosynthesis. Our data presented here and in the literature point to the
412 possibility that DosST modulate gene expression independently of DosR.

413 The synergy studies show significant synergistic interactions between artemisinin,
414 HC102A, HC103A, HC104, or HC106A. Moreover, artemisinin exhibited the greatest synergistic
415 activities with HC102A, HC103A or HC106A, indicating that inhibition of histidine kinases by a
416 second inhibitor can lead to synergistic inhibition of the DosRST pathway. This interaction could
417 be due to both sensor kinases being required for full induction of the DosR regulon, where DosT
418 responds early during hypoxia and DosS further induces the regulon at later times (39), and it is
419 possible that the inhibitors have different affinities for DosS or DosT. Thus, multiple inhibitors
420 could inhibit both DosS and DosT better than an inhibitor alone. Interestingly, artemisinin shows
421 the greatest synergism with HC106A. Both compounds are proposed to target the heme of
422 DosS/T, but through different mechanisms. This finding shows that both inhibitors can enter the
423 channel of DosST to interact with the heme and do so without antagonizing interactions.

424 The identification of new antibacterial agents and tuberculosis drugs has been associated
425 with the realization that these compounds can occupy a different region of chemical space relative
426 to drugs in most other therapeutic areas. Series HC106 is easily in the range of the characteristics
427 for compounds currently in use or in development as anti-TB compounds. Series HC104 needs
428 further exploration to fully assess its suitability. The physicochemical properties of a drug, such
429 as solubility and permeability, impact its oral bioavailability as these factors influence absorption,
430 distribution, metabolism, and excretion. Series HC106 demonstrates excellent aqueous solubility
431 (Table 2, with compounds generally having solubility >100 μM). The melting points of most of the
432 compounds in the series and the corresponding cLogP are also supportive appropriate solubility.

433 The ability of an anti-TB drug to reach its target site is greatly hampered by the highly impermeable
434 Mtb cell envelope. Both series (HC104 and HC106) demonstrate low micromolar and nanomolar
435 whole cell EC_{50} values, suggesting adequate cell wall permeability. SAR studies of HC106 show
436 that there remain significant opportunities for optimization of HC106 for potency and drug
437 properties and future studies will be focused on such optimizations.
438
439 **Methods**
440 ***Bacterial strains and growth conditions.*** Mtb CDC1551, CDC1551 (Δ*dosR*) strains were used
441 in this study. All cultures were grown at 37°C and 5% CO_2 in 7H9 Middlebrook medium
442 supplemented with 10% OADC (oleic acid albumin dextrose catalase) and 0.05% Tween-80 in
443 standing, vented tissue culture flasks, unless stated otherwise.
444
445 ***EC_{50} assays.*** The assay was performed as previously described (27). Briefly, the (*hspX'::GFP*)
446 reporter strain culture was diluted to an OD_{600} of 0.05 in fresh 7H9 media, pH 7.0, and 200 μL of
447 diluted culture was aliquoted in clear-bottom, black, 96-well plates (Corning). Cells were treated
448 with an 8-point (2.5-fold) dilution series ranging from 200 μM – 0.32 μM. For the structure
449 relationship studies for the HC106 series, a 12-point (2.5-fold) dilution series of HC106 analogs
450 ranging from 200 μM – 8.4 nM were used. GFP fluorescence and optical density were measured
451 following 6 d incubation. Percentage fluorescence and growth inhibitions were normalized to a
452 rifampin-positive control (100% inhibition) and DMSO-negative control (0% inhibition). EC_{50}
453 values were calculated for each compound using GraphPad Prism software package (version 6).
454 Each experiment was performed with two technical replicates per plate and two biological
455 replicates, and the error bar represents the s.d. of the biological replicates. Experiments were
456 performed twice with similar results.
457

458 ***Transcriptional profiling and data analysis.*** Transcriptional profiling studies were conducted
459 as previously described in Zheng *et al.* (27). Briefly, CDC1551 or CDC1551 (Δ*dosR*) cultures were
460 treated with 40 μM HC104A, HC106A or DMSO control for 6 d. The starting OD_{600} was 0.1 in 8
461 mL of 7H9 medium in standing T25 vented tissue culture flasks. Bacterial growth consumes
462 oxygen and stimulates the DosRST pathway. The total bacterial RNA from two biological
463 replicates was isolated and prepared for sequencing as previously described (40). The RNA-seq
464 data were processed and analyzed using the SPARTA software package (41).
465
466 ***Real time-PCR assays.*** The vitamin C and NO assays were performed as previously described
467 (27). Briefly, cultures at an OD_{600} of 0.6 were pretreated with 80 μM HC104A, HC106A or a DMSO
468 control for 24 h, and induced with 50 μM DETA-NONOate or 20 mM vitamin C for 2 h. For the
469 HC106A resistance assays, CDC1551 was transformed with the empty replicating plasmid pVV16
470 or the plasmid expressing *dosS* from the strong *hsp60* promoter (pVV16-DosS), and treated with
471 20 μM HC106A for 6 d. Total bacterial RNA was isolated and differential gene expression of
472 DosR-regulated genes, including *hspX* and *tgs1*, was quantified. The experiment was performed
473 in three technical replicates and error bars represent the s.d from the mean. The experiment was
474 repeated twice with similar results. To examine Mtb gene expression in macrophages, murine
475 bone-marrow derived macrophages were isolated as previously described (42) and seeded in
476 T75 vented, tissue culture flasks. Macrophages were infected with CDC1551 with multiplicity of
477 infection ratio of 1:20 as previously described (42). After infection, the flasks were treated with 40
478 μM HC104A or HC106A or DMSO for 48 h, with three individual flasks for each treatment. Total
479 bacterial RNA was isolated after treatment, and the transcripts of DosR-controlled genes (*hspX*
480 and *tgs1*) were quantified in RT-PCR. The experiment was conducted with three biological
481 replicates. The error bar represents the s.d. of the biological replicates.
482

483 ***TAG biosynthesis.*** The lipid labelling and TAG TLCs were performed as previously described
484 (27). Briefly, CDC1551 was cultured at an initial OD_{600} of 0.1 and radiolabeled with 8 μCi of [1,2-
485 ^{14}C] sodium acetate in T25 vented tissue culture flasks. The cultures were treated with 40 μM
486 HC104A, HC106A or DMSO for 6 d at 37°C. CDC1551 (Δ*dosR*) and *dosRS* complement strains
487 were also examined. Total lipids were extracted and ^{14}C incorporation was determined by
488 scintillation counting. 20,000 c.p.m. of total lipids were analyzed by TLC using silica gel 60
489 aluminum sheets (EMD Millipore). To determine TAG accumulation, the lipids were developed in
490 hexane-diethyl ether-acetic acid (80:20:1; vol/vol/vol) solvent system. The TLC was exposed to a
491 phosphor screen for 3 d, and imaged on a Typhoon imager and TAG was quantified using ImageJ
492 software (43). The experiment was repeated twice with similar results, and the error bar
493 represents the s.d. of two biological replicates.
494
495 ***NRP survival assays.*** Survival during NRP was examined using the hypoxic shift down assays
496 as previously described (27, 44). Briefly, CDC1551 cells were treated with 40 μM HC104A,
497 HC106A or DMSO control in a 24-well plate (1 mL/well). CDC1551 (Δ*dosR*) and *dosRS*
498 complement strains were also examined. Plates were incubated in an anaerobic chamber (BD
499 GasPak) for 12 d. It took 48 h for cultures to become anaerobic, as monitored by a methylene
500 blue control. Bacterial CFUs were numerated on 7H10 agar plates following incubation. The
501 experiment was repeated twice with similar results.
502
503 ***DosR protein purification.*** DosR full length protein was purified as previously described (45).
504 Briefly, the *dosR* gene (Rv3133c) was cloned into pET15b (Novagen Darmstadt, Germany) using
505 the primer set: forward primer 5'-TTTCATATGGTGGTAAAGGTCTTCTTGGTCGATGAC-3';
506 reverse primer 5'-TTTGGATCCTCATGGTCCATCACCGGGTGG-3'. The His_6-DosR protein was
507 expressed in *E. coli* BL21(DE3) strain. The culture was grown to OD_{600} 0.5-06, and induced with

508 1 mM IPTG for 6.5 h at 29°C. The cell pellet was suspended in lysis buffer (20 mM Tris-HCl, pH
509 8.0, 10% glycerol, 500 mM NaCl, 0.5 mg/ml lysozyme and 0.1 mg/ml PMSF), and incubated at
510 37°C for 30 min. The soluble fraction of lysate was collected after centrifugation and applied to a
511 TALON metal affinity Co^{2+} column (Clontech). The column was washed twice with washing buffer
512 (20 mM Tris-HCl, pH 8.0, 10% glycerol, 500 mM NaCl) without imidazole, then with 20 mM
513 imidazole. The protein was eluted with the same buffer containing 300 mM imidazole. The
514 fractions with the most DosR protein (as determined by SDS-PAGE) were pooled together for
515 dialysis in 25 mM Tris-HCl, pH 8.0. The final protein concentration was determined using a Qubit
516 kit (Invitrogen).
517
518 ***Electrophoretic mobility assay.*** The assay is fluorescence-based using 6-carboxyfluorescein
519 (6FAM) labeled 385 bp probe from the *hspX* promoter. In designing the primer set, 6FAM was
520 added to the 5' ends of forward and reverse primers. The *hspX* probe was synthesized via PCR
521 using the primer set: forward primer 5'-6FAM-CAACTGCACCGCGCTCTTGATG-3'; reverse
522 primer 5'-6FAM-CATCTCGTCTTCCAGCCGCATCAAC-3'. The probe was purified by Qiagen
523 PCR purification kit. The DosR protein was pre-phosphorylated in 10 μL of phosphorylation buffer
524 (40 mM Tris-HCl, pH 8.0, 5 mM $MgCl_2$, 50 mM lithium potassium acetyl phosphate), and incubated
525 at room temperature for 30 min. The protein was then transferred to binding buffer in a final
526 volume of 20 μL (final concentration, 25 mM Tris-HCl, pH 8.0, 0.5 mM EDTA, 20 mM KCl, 6 mM
527 $MgCl_2$, 10 nM probe, 1 μg poly-dI-dC (Sigma Aldrich)), and treated with HC104A or an equal
528 volume of DMSO or virstatin (Santa Cruz Biotech). Two different assays were performed. Firstly,
529 different DosR protein concentrations from 0.5 μM to 4 μM were treated with 40 μM. Second,
530 dose response assays were performed with 2 μM DosR treated with different concentrations of
531 HC104A or virstatin from 1 μM to 80 μM. After incubating on ice for 30 min, the reactions were
532 terminated by adding 1 μL 80% glycerol, and loaded on a native 5% Tris/Borate/EDTA (TBE)

533 polyacrylamide gel. The gel was run at 50 V, for 5-6 h at 4°C in 1X TBE buffer, and was imaged
534 using a Typhoon scanner with appropriate filters that can detect florescence at excitation = 495
535 nm, emission = 520 nm. Binding of the unbound probe was quantified using ImageJ (43). The
536 assay was repeated at least twice with similar results. The error bar represents the s.d. of two
537 biological replicates.
538
539 ***UV-visible spectroscopy assay.*** DosS and mutant proteins were purified and analyzed as
540 previously described (27). Briefly, 7.5 μM of recombinant DosS protein was deoxygenated with
541 argon gas in a sealed cuvette. The protein was reduced with 400 μM DTN for 20 min. The reaction
542 was then treated with 100 μM HC106A, 400 μM HC104A, 100 μM CORM-2
543 (tricarbonyldichlororuthenium (II) dimer) or equal volume of DMSO. The UV-visible spectra were
544 recorded for kinetic changes over 2 h. The experiment was repeated at least twice with similar
545 results.
546
547 ***Checkerboard synergy studies.*** The reporter strain CDC1551 (*hspX::GFP*) was treated with
548 pairs of DosRST inhibitors from 50 μM – 0.08 μM in 96-well plates, including HC101A-HC104A
549 and HC106A. GFP fluorescence and OD_{600} were measured after 6 d incubation. The percentage
550 of fluorescence inhibition (FI) and growth inhibition were calculated for each drug pair, with limited
551 growth inhibition observed. The FI data was utilized for further analysis of interactions using
552 CompuSyn software (34). The Combination Index (CI) value was calculated for each drug pair
553 according to the Chou-Talalay method, which is based on the Median-Effect equation derived
554 from the Mass-Action Law principle (35, 46). The resulting CI values provide quantitative
555 determination of drug interactions, including synergism (CI < 1), additive effect (C = 1), and
556 antagonism (C > 1).
557

558 ***Autophosphorylation assay.*** The DosS autophosphorylation assay was performed as
559 previously described (27). Recombinant DosS protein was treated with 10 μM, 20 μM or 40 μM
560 of HC104A, or HC106A. DMSO and 40 μM HC103A were also included as positive and negative
561 controls, respectively.
562
563 ***Kinetic solubility assay.*** The assay was performed with 7-point (2-fold) dilutions from 200 μM -
564 3.125 μM for HC106 analogs. Mebendazole, benxarotene and aspirin were also included as
565 controls. The drug dilutions were added to PBS, pH 7.4, with the final DMSO concentration of 1%,
566 and incubated at 37 °C for 2 h. The absorbance at 620 nm was measured for each drug dilution
567 to estimate of the compound solubility. Three replicates were examined for each dilution.
568
569 **Acknowledgements**
570 The MSU RTSF provided technical support for the RNA-seq library preparation and sequencing.
571 This project was supported by start-up funding and a Molecular Discovery Grant from Michigan
572 State University, AgBioResearch, a grant from the NIH-NIAID (R21AI105687) and Grand
573 Challenges Explorations grants from the Bill and Melinda Gates Foundation (OPP1059227 and
574 OPP1119065).
575
576 **Author Contributions**
577 H.Z., E.E. and R.B.A conceived the experiments. H.Z. performed the Mtb physiology and
578 biochemistry experiments. B.A. synthesized the analogs. E.E. directed the medicinal chemistry
579 optimizations. H.Z, E.E. and R.B.A wrote the manuscript.
580 **Disclosures**
581 RBA is the founder and owner of Tarn Biosciences, Inc., a company that is working to develop
582 new TB drugs.

583 **References**
584

585 1. Boon C & Dick T (2012) How *Mycobacterium tuberculosis* goes to sleep: the dormancy
586 survival regulator DosR a decade later. *Future microbiology* 7(4):513-518.
587 2. Rustad TR, Sherrid AM, Minch KJ, & Sherman DR (2009) Hypoxia: a window into
588 Mycobacterium tuberculosis latency. *Cell Microbiol* 11(8):1151-1159.
589 3. Wayne LG & Sohaskey CD (2001) Nonreplicating persistence of mycobacterium
590 tuberculosis. *Annu Rev Microbiol* 55:139-163.
591 4. Mehra S*, et al.* (2015) The DosR Regulon Modulates Adaptive Immunity and Is Essential
592 for Mycobacterium tuberculosis Persistence. *American journal of respiratory and critical*
593 *care medicine* 191(10):1185-1196.
594 5. Hudock TA*, et al.* (2017) Hypoxia sensing and persistence genes are expressed during
595 the intragranulomatous survival of *Mycobacterium tuberculosis*. *American journal of*
596 *respiratory cell and molecular biology* 56(5):637-647.
597 6. Dasgupta N*, et al.* (2000) Characterization of a two-component system, devR-devS, of
598 *Mycobacterium tuberculosis*. *Tubercle and lung disease : the official journal of the*
599 *International Union against Tuberculosis and Lung Disease* 80(3):141-159.
600 7. Park HD*, et al.* (2003) Rv3133c/dosR is a transcription factor that mediates the hypoxic
601 response of Mycobacterium tuberculosis. *Mol Microbiol* 48(3):833-843.
602 8. Saini DK*, et al.* (2004) DevR-DevS is a bona fide two-component system of
603 *Mycobacterium tuberculosis* that is hypoxia-responsive in the absence of the DNA-
604 binding domain of DevR. *Microbiology (Reading, England)* 150(Pt 4):865-875.
605 9. Voskuil MI*, et al.* (2003) Inhibition of respiration by nitric oxide induces a Mycobacterium
606 tuberculosis dormancy program. *J Exp Med* 198(5):705-713.
607 10. Kumar A*, et al.* (2008) Heme oxygenase-1-derived carbon monoxide induces the
608 Mycobacterium tuberculosis dormancy regulon. *J Biol Chem* 283(26):18032-18039.
609 11. Lee JM*, et al.* (2008) O2- and NO-sensing mechanism through the DevSR two-
610 component system in *Mycobacterium smegmatis*. *Journal of bacteriology* 190(20):6795-
611 6804.
612 12. Sousa EH, Tuckerman JR, Gonzalez G, & Gilles-Gonzalez MA (2007) DosT and DevS
613 are oxygen-switched kinases in *Mycobacterium tuberculosis*. *Protein science : a*
614 *publication of the Protein Society* 16(8):1708-1719.
615 13. Kumar A, Toledo JC, Patel RP, Lancaster JR, Jr., & Steyn AJ (2007) Mycobacterium
616 tuberculosis DosS is a redox sensor and DosT is a hypoxia sensor. *Proc Natl Acad Sci*
617 *U S A* 104(28):11568-11573.
618 14. Ioanoviciu A, Yukl ET, Moenne-Loccoz P, & de Montellano PR (2007) DevS, a heme-
619 containing two-component oxygen sensor of *Mycobacterium tuberculosis*. *Biochemistry*
620 46(14):4250-4260.
621 15. Kim MJ, Park KJ, Ko IJ, Kim YM, & Oh JI (2010) Different roles of DosS and DosT in the
622 hypoxic adaptation of Mycobacteria. *J Bacteriol* 192(19):4868-4875.
623 16. Rao SP, Alonso S, Rand L, Dick T, & Pethe K (2008) The protonmotive force is required
624 for maintaining ATP homeostasis and viability of hypoxic, nonreplicating Mycobacterium
625 tuberculosis. *Proc Natl Acad Sci U S A* 105(33):11945-11950.
626 17. Adams KN*, et al.* (2011) Drug tolerance in replicating mycobacteria mediated by a
627 macrophage-induced efflux mechanism. *Cell* 145(1):39-53.
628 18. Grant SS, Kaufmann BB, Chand NS, Haseley N, & Hung DT (2012) Eradication of
629 bacterial persisters with antibiotic-generated hydroxyl radicals. *Proceedings of the*
630 *National Academy of Sciences of the United States of America* 109(30):12147-12152.
631 19. Leistikow RL*, et al.* (2010) The Mycobacterium tuberculosis DosR regulon assists in
632 metabolic homeostasis and enables rapid recovery from nonrespiring dormancy. *J*
633 *Bacteriol* 192(6):1662-1670.

634 20. Converse PJ*, et al.* (2009) Role of the dosR-dosS two-component regulatory system in
635 Mycobacterium tuberculosis virulence in three animal models. *Infect Immun* 77(3):1230-
636 1237.
637 21. Gautam US, Mehra S, & Kaushal D (2015) *in-vivo* gene signatures of *Mycobacterium*
638 *tuberculosis* in C3HeB/FeJ Mice. *PloS one* 10(8):e0135208.
639 22. Gautam US*, et al.* (2015) DosS is required for the complete virulence of *Mycobacterium*
640 *tuberculosis* in mice with classical granulomatous lesions. *American journal of*
641 *respiratory cell and molecular biology* 52(6):708-716.
642 23. Deb C*, et al.* (2009) A novel in vitro multiple-stress dormancy model for Mycobacterium
643 tuberculosis generates a lipid-loaded, drug-tolerant, dormant pathogen. *Plos One*
644 4(6):e6077.
645 24. Basak A*, et al.* (2017) Antimicrobial peptide-inspired NH125 analogues: bacterial and
646 fungal biofilm-eradicating agents and rapid killers of MRSA persisters. *Organic &*
647 *biomolecular chemistry* 15(26):5503-5512.
648 25. Abramovitch RB (2018) Mycobacterium tuberculosis Reporter Strains as Tools for Drug
649 Discovery and Development. *IUBMB Life* 70(9):818-825.
650 26. Johnson BK & Abramovitch RB (2017) Small Molecules That Sabotage Bacterial
651 Virulence. *Trends in pharmacological sciences* 38(4):339-362.
652 27. Zheng H*, et al.* (2017) Inhibitors of Mycobacterium tuberculosis DosRST signaling and
653 persistence. *Nature chemical biology* 13(2):218-225.
654 28. Daniel J*, et al.* (2004) Induction of a novel class of diacylglycerol acyltransferases and
655 triacylglycerol accumulation in *Mycobacterium tuberculosis* as it goes into a dormancy-
656 like state in culture. *Journal of bacteriology* 186(15):5017-5030.
657 29. Sirakova TD*, et al.* (2006) Identification of a diacylglycerol acyltransferase gene involved
658 in accumulation of triacylglycerol in *Mycobacterium tuberculosis* under stress.
659 *Microbiology (Reading, England)* 152(Pt 9):2717-2725.
660 30. Baek SH, Li AH, & Sassetti CM (2011) Metabolic regulation of mycobacterial growth and
661 antibiotic sensitivity. *PLoS Biol* 9(5):e1001065.
662 31. Hung DT, Shakhnovich EA, Pierson E, & Mekalanos JJ (2005) Small-molecule inhibitor
663 of Vibrio cholerae virulence and intestinal colonization. *Science* 310(5748):670-674.
664 32. Podust LM, Ioanoviciu A, & Ortiz de Montellano PR (2008) 2.3 A X-ray structure of the
665 heme-bound GAF domain of sensory histidine kinase DosT of Mycobacterium
666 tuberculosis. *Biochemistry* 47(47):12523-12531.
667 33. Cho HY, Cho HJ, Kim YM, Oh JI, & Kang BS (2009) Structural insight into the heme-
668 based redox sensing by DosS from Mycobacterium tuberculosis. *J Biol Chem*
669 284(19):13057-13067.
670 34. Chou T & Martin N (2005) CompuSyn for drug combinations: PC software and user's
671 guide: a computer program for quantitation of synergism and antagonism in drug
672 combinations, and the determination of IC50 and ED50 and LD50 values).
673 35. Chou TC & Talalay P (1984) Quantitative analysis of dose-effect relationships: the
674 combined effects of multiple drugs or enzyme inhibitors. *Adv Enzyme Regul* 22:27-55.
675 36. Boulton AJ & Katritzky AR (1961) The tautomerism of heteroaromatic compounds with
676 five-membered rings—I: 5-hydroxyisoxazoles-isoxazol-5-ones. *Tetrahedron* 12(1):41-50.
677 37. Topliss JG (1972) Utilization of operational schemes for analog synthesis in drug design.
678 *Journal of medicinal chemistry* 15(10):1006-1011.
679 38. Lee HN, Jung KE, Ko IJ, Baik HS, & Oh JI (2012) Protein-protein interactions between
680 histidine kinases and response regulators of *Mycobacterium tuberculosis* H37Rv.
681 *Journal of microbiology (Seoul, Korea)* 50(2):270-277.
682 39. Honaker RW, Leistikow RL, Bartek IL, & Voskuil MI (2009) Unique roles of DosT and
683 DosS in DosR regulon induction and Mycobacterium tuberculosis dormancy. *Infect*
684 *Immun* 77(8):3258-3263.

685 40. Baker JJ, Johnson BK, & Abramovitch RB (2014) Slow growth of Mycobacterium
686 tuberculosis at acidic pH is regulated by phoPR and host-associated carbon sources.
687 *Mol Microbiol* 94(1):56-69.
688 41. Johnson BK, Scholz MB, Teal TK, & Abramovitch RB (2016) SPARTA: Simple Program
689 for Automated reference-based bacterial RNA-seq Transcriptome Analysis. *BMC*
690 *bioinformatics* 17:66.
691 42. Johnson BK & Abramovitch RB (2015) Macrophage Infection Models for Mycobacterium
692 tuberculosis. *Methods Mol Biol* 1285:329-341.
693 43. Schneider CA, Rasband WS, & Eliceiri KW (2012) NIH Image to ImageJ: 25 years of
694 image analysis. *Nature methods* 9(7):671-675.
695 44. Mak PA*, et al.* (2012) A high-throughput screen to identify inhibitors of ATP homeostasis
696 in non-replicating Mycobacterium tuberculosis. *ACS chemical biology* 7(7):1190-1197.
697 45. Vashist A, Prithvi Raj D, Gupta UD, Bhat R, & Tyagi JS (2016) The alpha10 helix of
698 DevR, the *Mycobacterium tuberculosis* dormancy response regulator, regulates its DNA
699 binding and activity. *The FEBS journal* 283(7):1286-1299.
700 46. Chou TC (2010) Drug combination studies and their synergy quantification using the
701 Chou-Talalay method. *Cancer research* 70(2):440-446.
702
703

704 **Figure Legends**
705
706 **Figure 1. HC104A and HC106A inhibit DosRST reporter fluorescence.** (**a**) Chemical structures of
707 HC104A and HC106A. HC104A (**b**) and HC106A (**c**) inhibited DosR-driven GFP fluorescence
708 signal in a dose-dependent manner, while having minimal impact of Mtb growth. The EC_{50} values
709 of fluorescence inhibition for HC104A and HC106A are 9.8 μM and 2.5 μM, respectively.
710
711 **Figure 2. Transcriptional profiling shows HC104A and HC106A inhibited DosR regulon during**
712 **hypoxia.** Magnitude-amplitude plots showing differential gene expression of Mtb cells treated with
713 40 μM HC104A (**a**) or HC106A (**b**). The labeled genes represent selected genes that belong to
714 the DosRST regulon. The red dots represent genes with significant differential expression, q<0.05.
715 **(c)** A Venn diagram for the downregulated genes (>2-fold; q< 0.05) of WT CDC1551 treated with
716 HC104A or HC106A compared to that of CDC1551 (Δ*dosR*). (**d**) Venn diagram for downregulated
717 genes (>2-fold; q< 0.05) of CDC1551 (Δ*dosR*) treated with HC104A or HC106A.
718
719 **Figure 3. Inhibition of DosR regulon and persistence-associated physiologies by HC104A and**
720 **HC106A.** (**a**) Inhibition of DosR regulon in murine macrophages infected with Mtb and treated with
721 HC104A and HC106A for 48 h. Bacterial RNA was isolated after incubation, and the differential
722 gene expression of *hspX* and *tgs1* bone-marrow derived were quantified by qRT-PCR. The error
723 bars represent the standard derivation of three biological replicates. (**b**) HC104A and HC106A
724 inhibit DosR regulon induction by vitamin C and NO. Cells were pretreated with the compounds
725 or DMSO for 24 h, and induced with vitamin C or NO for 2 h. Total bacterial RNA was isolated,
726 and the transcripts of DosR-regulated genes, *hspX* and *tgs1*, were quantified by qRT-PCR. The
727 difference in the drug treated samples compared to DMSO treated samples in response to vitamin
728 C or NO are significant with a p-value <0.001 based on a t-test, except the one marked as non-
729 significant (n.s.). The error bars represent the standard deviation of three replicates. The

730 experiment was repeated twice with similar results. (**c**) Inhibition of TAG accumulation of Mtb
731 treated with HC104A or HC106A. Mtb cells were treated with 40 μM of the compounds and labeled
732 with [1,2-^{14}C] sodium acetate for 6 d. Total lipid was isolated and analyzed by TLC. TAG
733 accumulation was quantified from the TLC. The error bars represent the standard derivation of
734 two biological replicates. (**d**) Mtb cell survival during NRP when treated with HC104A or HC106A
735 during NRP. Mtb cells were pretreated with 40 μM of compounds for 48 h in an anaerobic
736 chamber, and continued incubation for 10 d. Surviving bacteria were enumerated on 7H10 agar.
737 The error bars represent the standard derivation of three biological replicates. The experiment
738 was repeated twice with similar results.
739
740 **Figure 4. Inhibition of DosR DNA-binding by HC104A.** (**a**) DosR protein ranging from 0.5 μM
741 to 4 μM was treated with DMSO or 40 μM HC104A and binding to the *hspX* promoter was
742 examined by EMSA. HC104A inhibits DosR DNA binding at 2 μM concentration. (**b**) The free DNA
743 of each reaction was quantified in ImageJ and the percentage of free DNA was normalized using
744 reactions containing 0.5 μM DosR as 100% free DNA. Differences between reactions containing
745 2 μM DosR treated with DMSO or HC104A are significant (**P value <0.005 based on a t-test).
746 The error bars represent the standard derivation of two biological replicates. (**c**) Dose-dependent
747 impact of HC104A on DosR DNA binding. DosR protein at 2 μM was treated with HC104A at
748 concentrations from 1 μM to 80 μM. (**c**) The free DNA of each reaction was also quantified in
749 ImageJ with the percentage of free DNA is normalized using the reaction containing 80 μM
750 HC104A as 100% free DNA. The differences between treated reactions as compared to DMSO
751 control are significant. (*P value <0.05 and **P value <0.005 based on a t-test). The error bars
752 represent the standard derivation of two biological reps.
753

754 **Figure 5. Interactions between HC106A and DosS heme.** WT DosS protein was treated with
755 dithionite (DTN) and then 100 μM HC106A (**a**) or 100 μM pf CORM-2 (a CO donor) (**b**). The UV-
756 visible spectra of the two treatments exhibited a shift of the Soret peak to a common position of
757 422 nm. (**c**) DosS with a G117L amino acid substitution, that is predicted to block the heme
758 exposing channel, provides resistance to HC106A. The spectrum of the mutant protein did not
759 change, after HC106A treatment, indicating resistance to HC106A. (**d**) Overexpression of DosS
760 protein promotes resistance to HC106A treatment in Mtb. Mtb cells with the pVV16 empty vector
761 or the DosS overexpression plasmid were treated with 20 μM HC106A for 6 d. Bacterial RNA was
762 isolated for analysis of the differential gene expression of *hspX* and *tgs1* and analyzed by qRT-
763 PCR. Overexpression of DosS caused 23- and 16.5-fold increase of *hspX* and *tgs1* transcripts,
764 respectively, compared to the empty vector control (***P value <0.0001 based on a *t*-test). The
765 error bar represents the standard derivation of the mean for three technical replicates. The
766 experiments were repeated twice with a similar result.
767
768 **Figure 6. Synergistic interactions between DosRST inhibitors.** CDC1551 (*hspX'::GFP*) was treated
769 with pairwise combinations of two compounds at concentrations of 50 μM to 0.08 μM. GFP
770 fluorescence was measured and used to calculate percentage inhibition. The data were analyzed
771 in the CompuSyn software to determine the combination index (CI) for the panel of each drug
772 combination, including (**a**) artemisinin and HC102A; (**b**) artemisinin and HC103A; (**c**) artemisinin
773 and HC104A; and (**d**) artemisinin and HC106A. Example EC_{50} curves are presented with
774 individual compounds or a selected synergistic combination to illustrate the potentiating
775 interactions.
776
777 **Table 1. Initial SAR studies of the HC106 series. The HC106 analogs with different R-**
778 **groups were synthesized or purchased. The reporter strain CDC1551 (*hspX'::GFP*) was**

779 **treated with across doses of each analog from 200 μM to 0.328 μM. The EC_{50} values of**

780 **fluorescence inhibition calculated for each analog to determine their potency.**

781

782 **Table 2. Early SAR studies of "A-ring" analogs of HC106.** The HC106 analogs with different

783 R-groups were synthesized. The reporter strain CDC1551 (*hspX'::GFP*) was treated with across

784 doses of each analog from 200 μM to 0.328 μM. The EC_{50} values of fluorescence inhibition

785 were calculated for each analog to determine their potency. The other chemical properties of the

786 analogs are also included. Kinetic solubility and mouse microsomal stability were both

787 experimentally determined.

788

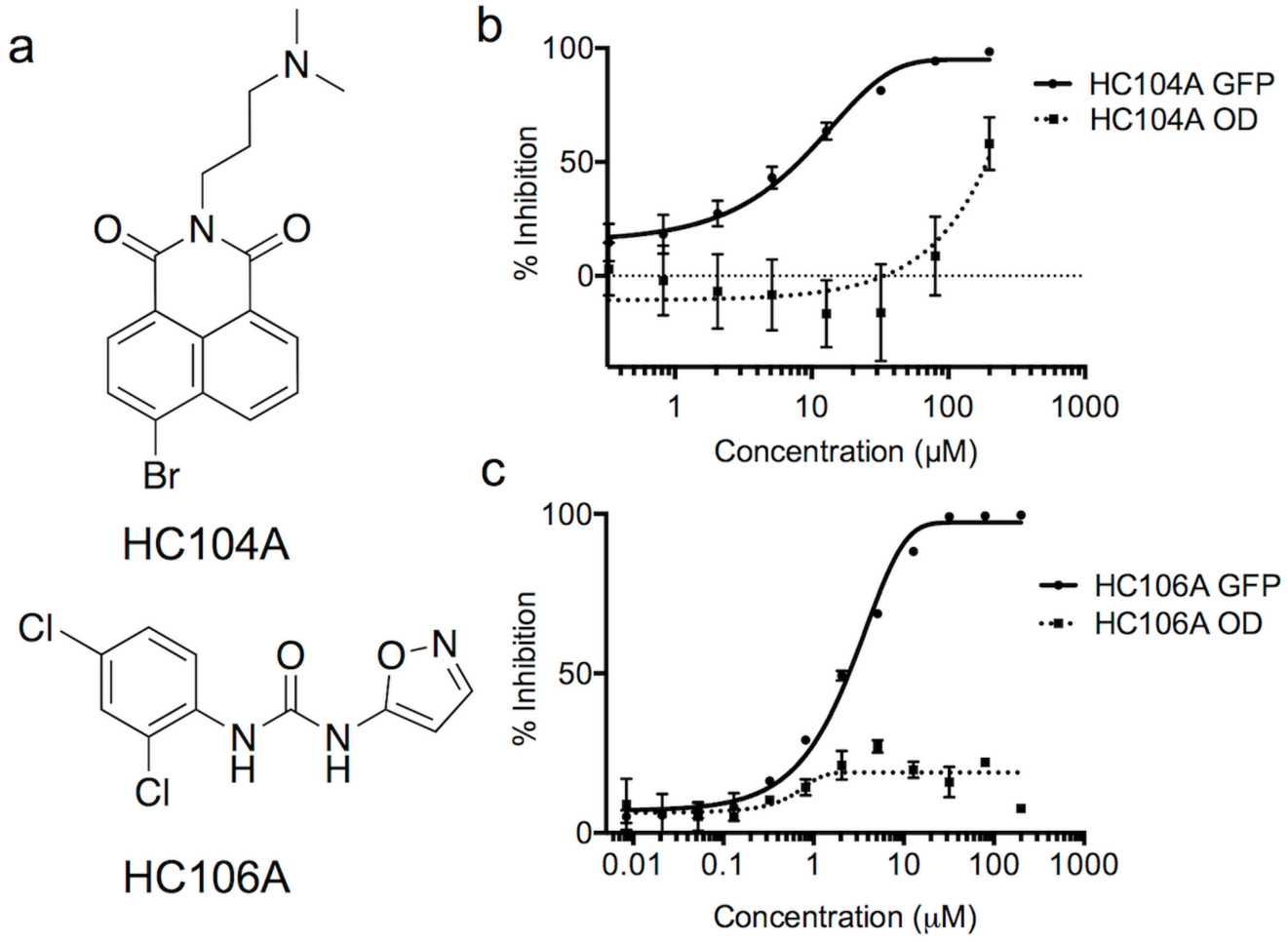
a
N
O
N
O
Br
HC104A
Cl
O
O
N
N
H
N
H
Cl
HC106A
b
100
50
0
% Inhibition
1
10
100
1000
Concentration (μM)
HC104A GFP
HC104A OD
c
100
50
0
% Inhibition
0.01
0.1
1
10
100
1000
Concentration (μM)
HC106A GFP
HC106A OD

Figure 1

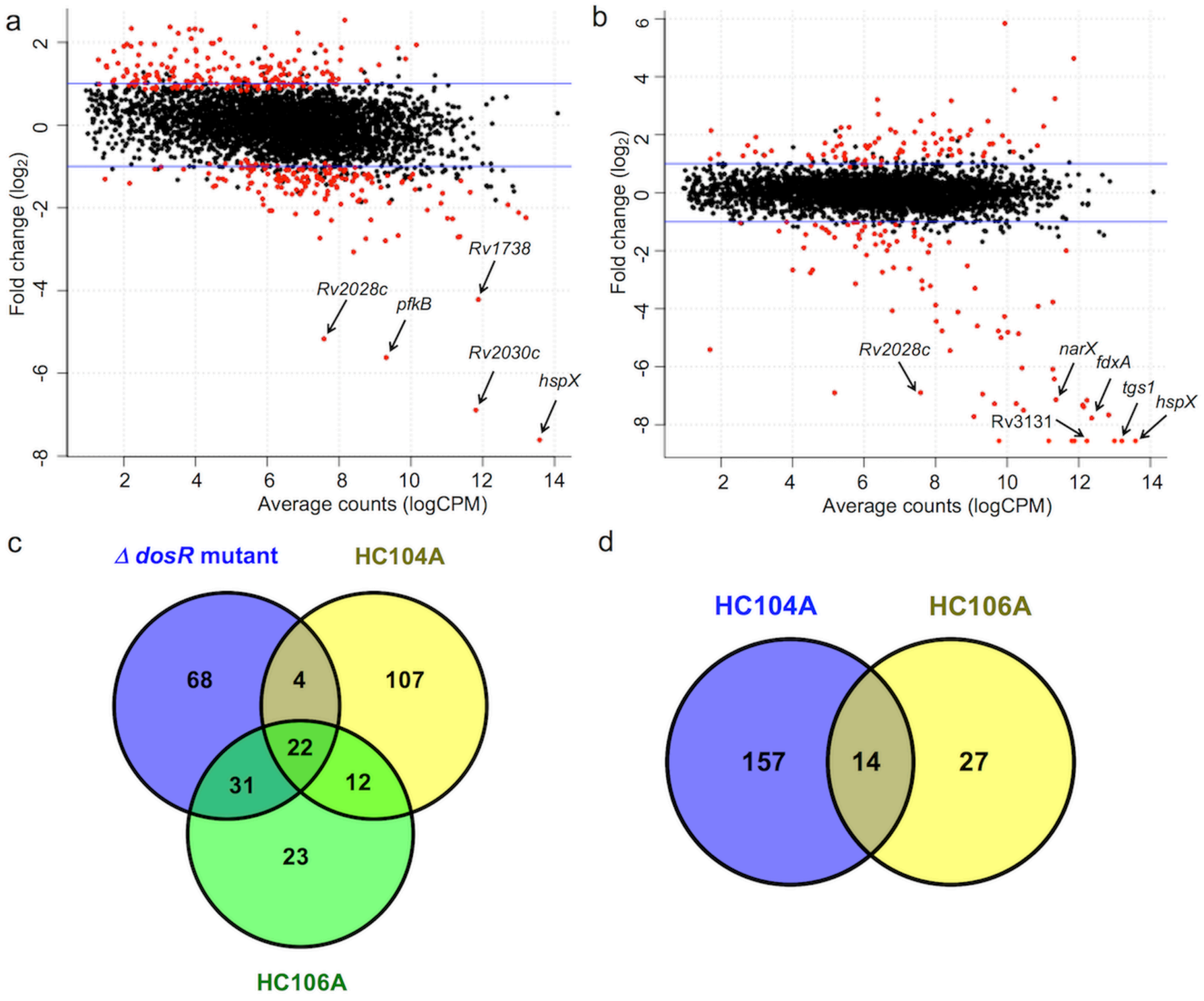
a
Fold change (log2)
Average counts (logCPM)
Rv1738
Rv2028c
pfkB
Rv2030c
hspX
b
Fold change (log2)
Average counts (logCPM)
Rv2028c
narX
fdxA
tgs1
hspX
Rv3131
c
Δ dosR mutant
HC104A
HC106A
68
4
107
22
31
12
23
d
HC104A
HC106A
157
14
27

Figure 2

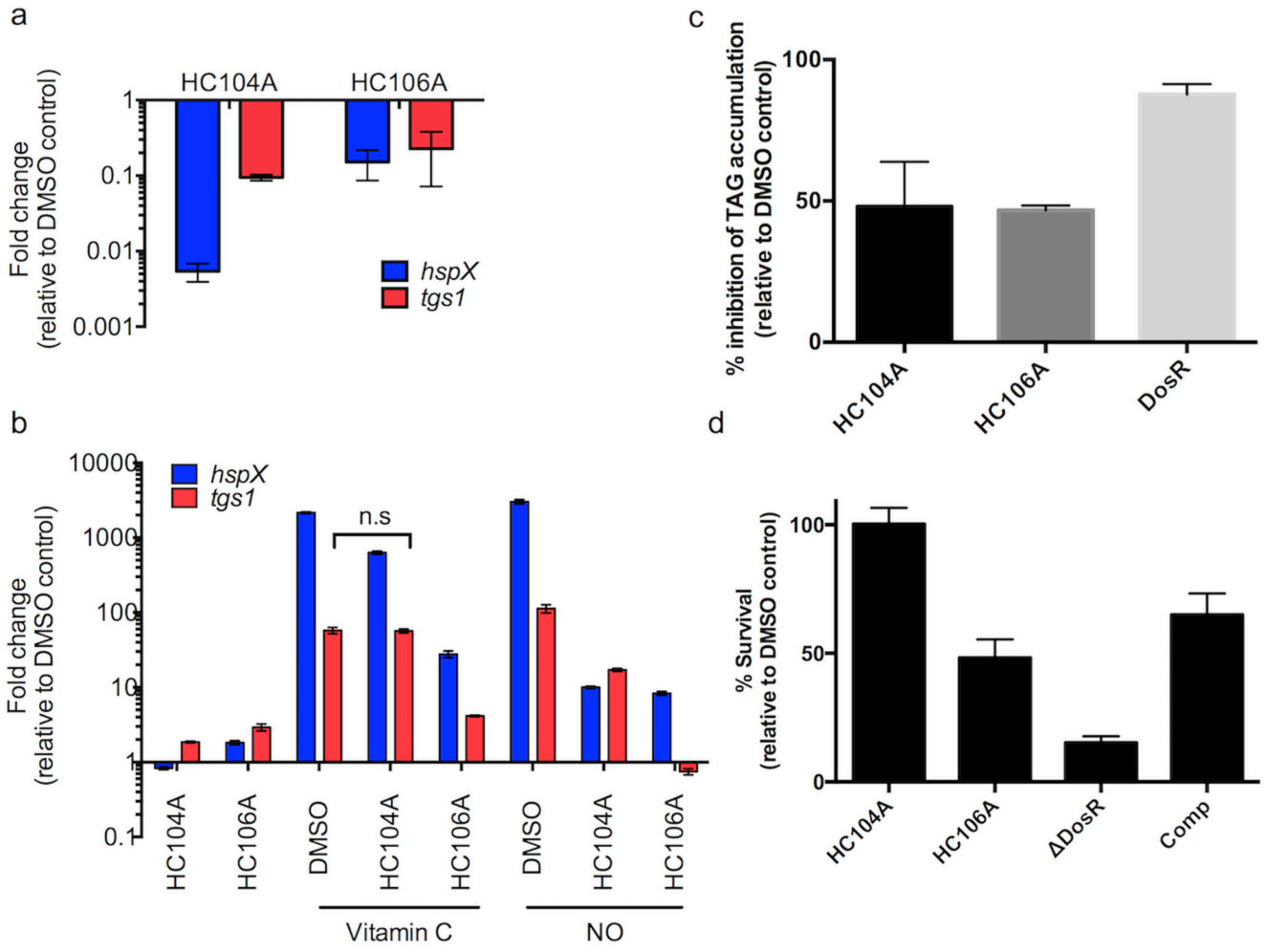
a
HC104A
HC106A
Fold change
(relative to DMSO control)
1
0.1
0.01
0.001
hspX
tgs1
b
10000
1000
100
10
1
0.1
hspX
tgs1
n.s
Fold change
(relative to DMSO control)
HC104A
HC106A
DMSO
HC104A
HC106A
DMSO
HC104A
HC106A
Vitamin C
NO
c
% inhibition of TAG accumulation
(relative to DMSO control)
100
50
0
HC104A
HC106A
DosR
d
% Survival
(relative to DMSO control)
100
50
0
HC104A
HC106A
ΔDosR
Comp

Figure 3

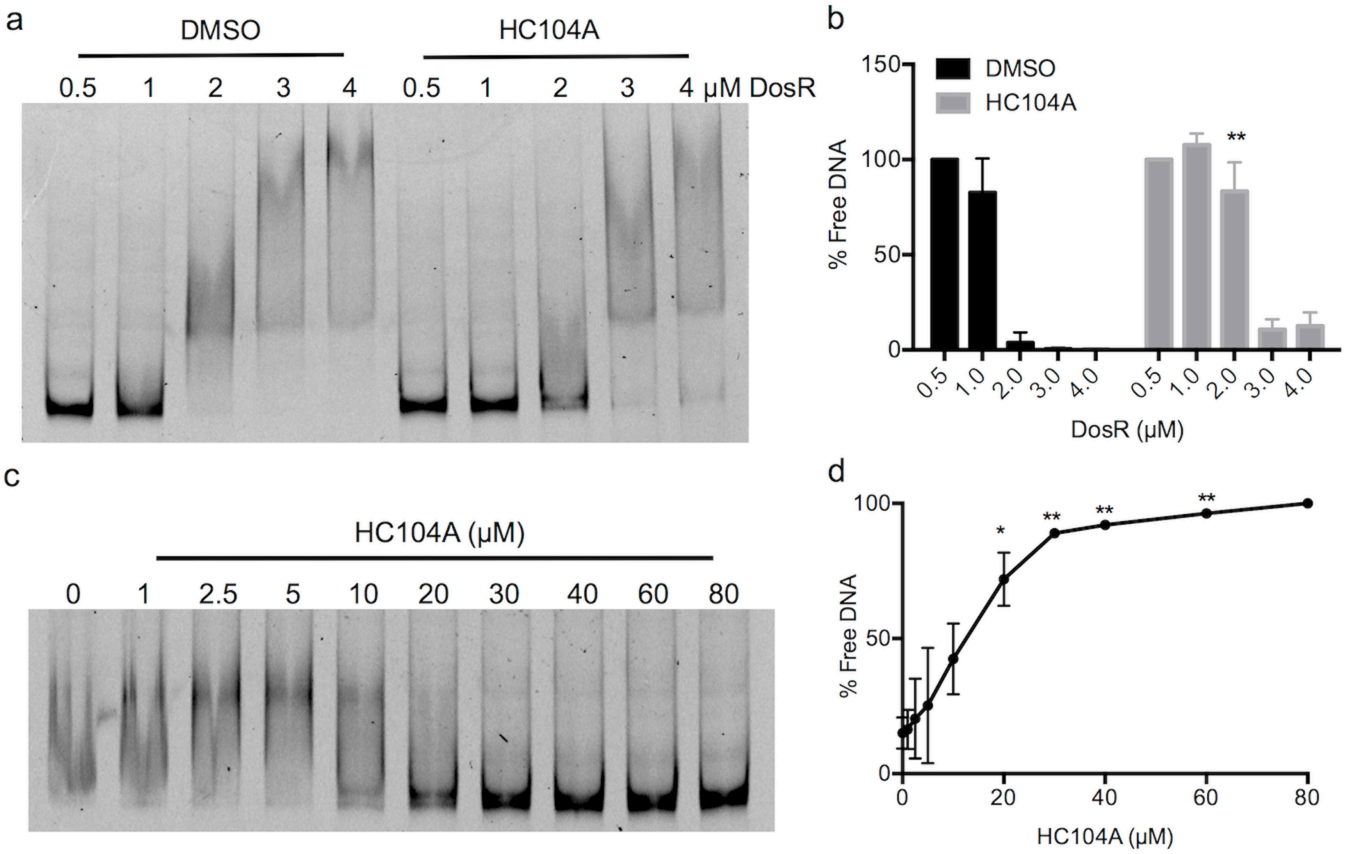
a
DMSO
HC104A
0.5 1 2 3 4 0.5 1 2 3 4 μM DosR
b
DMSO
HC104A
% Free DNA
150
100
50
0
**
0.5 1.0 2.0 3.0 4.0 0.5 1.0 2.0 3.0 4.0
DosR (μM)
c
HC104A (μM)
0 1 2.5 5 10 20 30 40 60 80
d
% Free DNA
100
50
0
*
**
**
**
0 20 40 60 80
HC104A (μM)

Figure 4

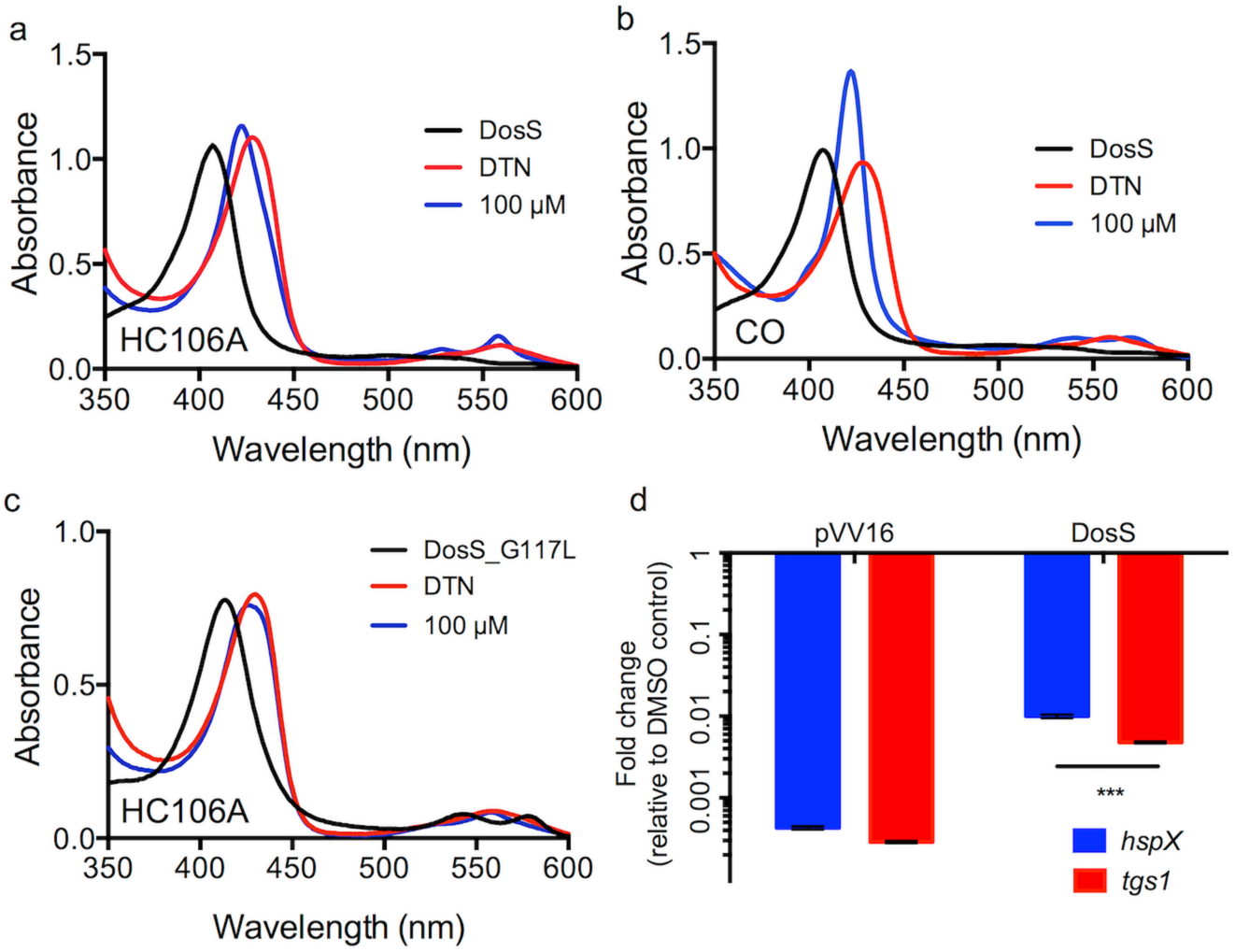
a
Absorbance
1.5
1.0
0.5
0.0
HC106A
DosS
DTN
100 μM
350
400
450
500
550
600
Wavelength (nm)
b
Absorbance
1.5
1.0
0.5
0.0
CO
DosS
DTN
100 μM
350
400
450
500
550
600
Wavelength (nm)
c
Absorbance
1.0
0.5
0.0
HC106A
DosS_G117L
DTN
100 μM
350
400
450
500
550
600
Wavelength (nm)
d
pVV16
DosS
Fold change
(relative to DMSO control)
1
0.1
0.01
0.001
***
hspX
tgs1

Figure 5

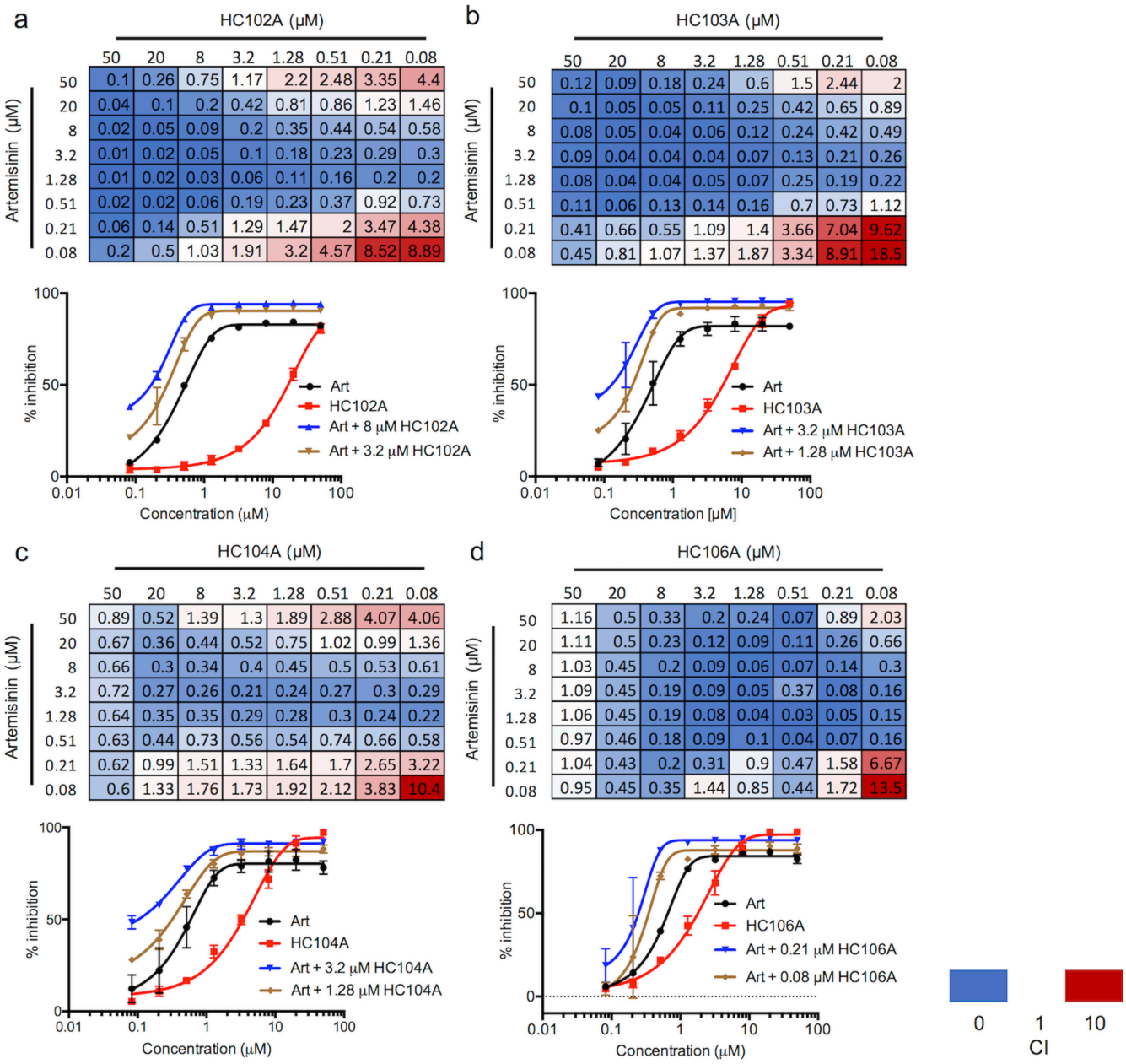
a
HC102A (μM)
50 20 8 3.2 1.28 0.51 0.21 0.08
Artemisinin (μM)
50 0.1 0.26 0.75 1.17 2.2 2.48 3.35 4.4
20 0.04 0.1 0.2 0.42 0.81 0.86 1.23 1.46
8 0.02 0.05 0.09 0.2 0.35 0.44 0.54 0.58
3.2 0.01 0.02 0.05 0.1 0.18 0.23 0.29 0.3
1.28 0.01 0.02 0.03 0.06 0.11 0.16 0.2 0.2
0.51 0.02 0.02 0.06 0.19 0.23 0.37 0.92 0.73
0.21 0.06 0.14 0.51 1.29 1.47 2 3.47 4.38
0.08 0.2 0.5 1.03 1.91 3.2 4.57 8.52 8.89
% inhibition
Concentration (μM)
Art
HC102A
Art + 8 μM HC102A
Art + 3.2 μM HC102A
b
HC103A (μM)
50 20 8 3.2 1.28 0.51 0.21 0.08
Artemisinin (μM)
50 0.12 0.09 0.18 0.24 0.6 1.5 2.44 2
20 0.1 0.05 0.05 0.11 0.25 0.42 0.65 0.89
8 0.08 0.05 0.04 0.06 0.12 0.24 0.42 0.49
3.2 0.09 0.04 0.04 0.04 0.07 0.13 0.21 0.26
1.28 0.08 0.04 0.04 0.05 0.07 0.25 0.19 0.22
0.51 0.11 0.06 0.13 0.14 0.16 0.7 0.73 1.12
0.21 0.41 0.66 0.55 1.09 1.4 3.66 7.04 9.62
0.08 0.45 0.81 1.07 1.37 1.87 3.34 8.91 18.5
% inhibition
Concentration [μM]
Art
HC103A
Art + 3.2 μM HC103A
Art + 1.28 μM HC103A
c
HC104A (μM)
50 20 8 3.2 1.28 0.51 0.21 0.08
Artemisinin (μM)
50 0.89 0.52 1.39 1.3 1.89 2.88 4.07 4.06
20 0.67 0.36 0.44 0.52 0.75 1.02 0.99 1.36
8 0.66 0.3 0.34 0.4 0.45 0.5 0.53 0.61
3.2 0.72 0.27 0.26 0.21 0.24 0.27 0.3 0.29
1.28 0.64 0.35 0.35 0.29 0.28 0.3 0.24 0.22
0.51 0.63 0.44 0.73 0.56 0.54 0.74 0.66 0.58
0.21 0.62 0.99 1.51 1.33 1.64 1.7 2.65 3.22
0.08 0.6 1.33 1.76 1.73 1.92 2.12 3.83 10.4
% inhibition
Concentration (μM)
Art
HC104A
Art + 3.2 μM HC104A
Art + 1.28 μM HC104A
d
HC106A (μM)
50 20 8 3.2 1.28 0.51 0.21 0.08
Artemisinin (μM)
50 1.16 0.5 0.33 0.2 0.24 0.07 0.89 2.03
20 1.11 0.5 0.23 0.12 0.09 0.11 0.26 0.66
8 1.03 0.45 0.2 0.09 0.06 0.07 0.14 0.3
3.2 1.09 0.45 0.19 0.09 0.05 0.37 0.08 0.16
1.28 1.06 0.45 0.19 0.08 0.04 0.03 0.05 0.15
0.51 0.97 0.46 0.18 0.09 0.1 0.04 0.07 0.16
0.21 1.04 0.43 0.2 0.31 0.9 0.47 1.58 6.67
0.08 0.95 0.45 0.35 1.44 0.85 0.44 1.72 13.5
% inhibition
Concentration (μM)
Art
HC106A
Art + 0.21 μM HC106A
Art + 0.08 μM HC106A
0 1 10
CI

Figure 6

ID#	Compound	EC_{50} (μM)	ID#	Compound	EC_{50} (μM)
HC106F	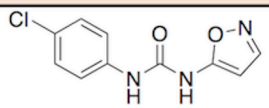	1.33	MSU-41324	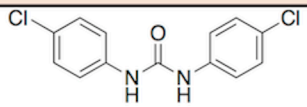	>200
HC106A	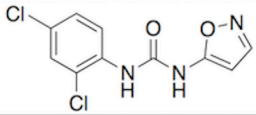	2.48	MSU-39449	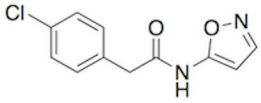	5.2
HC106C	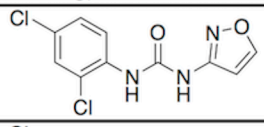	>200	MSU-39451	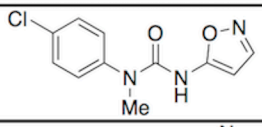	4.14
MSU-39450	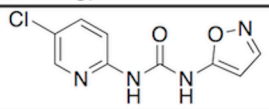	1.95	MSU-39453	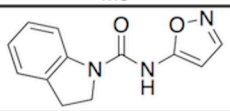	16.62
MSU-39444	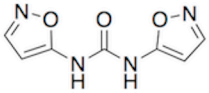	1.7	MSU-41422	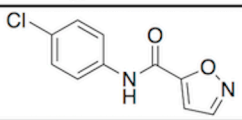	>200
MSU-41425	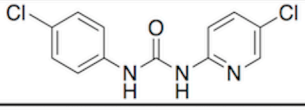	>200			

Table 1

	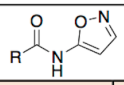								
ID#	Compound R =	EC_{50} (μM)	MW (g/mol)	TPSA (ang^2)	Ligand Efficiency (LE)	m.p. (°C)	cLogP	Solubility (μM)	Microsomes (% remaining @ 30 minutes)
HC106F	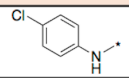	1.33	237.6	63	0.50	183	2.2	>200	115%
HC106A	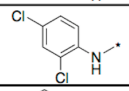	2.48	272.1	63	0.41	164	2.7	110	-
MSU-33189		0.63	203.1	63	0.56	183-184	1.6	-	-
MSU-39447	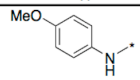	0.61	233.2	72	0.49	166-167	1.5	>100	-
MSU-39448	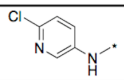	1.42	238.6	75	0.49	158-159	1.3	-	-
MSU-39450	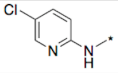	1.95	238.6	75	0.38	122-123	1.3	-	-
MSU-39446	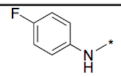	0.54	221.2	63	0.52	176-177	1.7	>100	70%
MSU-41464	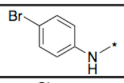	1.2	282.1	67	0.51	183-184	2.3	-	109%
MSU-39445	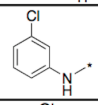	0.75	237.6	63	0.52	159 (dec)	2.1	>100	-
MSU-39452	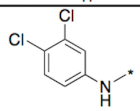	2.47	272.1	63	0.45	164	2.8	-	-
MSU-41442	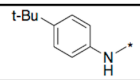	2.08	259.3	63	0.41	163	3.1	>100	-
MSU-41443	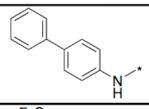	11.2	279.3	63	0.32	193	3.2	14	-
MSU-41463	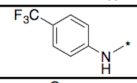	1.67	271.2	67	0.42	178	2.4	-	84
MSU-41465	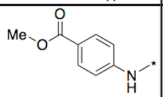	1.16	261.2	94	0.43	194	1.5	-	73
MSU-41462	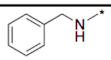	1.12	217.2	67	0.45	128-130	1.3	-	-
MSU-41542	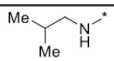	1.34	183.2	67	0.62	187	0.9	-	-
MSU-41545	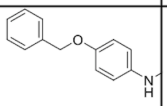	4.75	309.3	76	0.32	164	2.9	-	-
MSU-41546		2.15	195.2	67	0.56	182	1.1	-	-
MSU-42002		1.21	209.2	67	0.54	180	1.4	-	-
MSU-42003	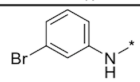	1.94	282.1	67	0.49	157	2.3	-	-
MSU-42004	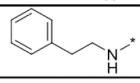	2.36	231.3	67	0.45	165	1.7	-	-

Table 2

Supplementary Methods and Figures

Inhibition of *Mycobacterium tuberculosis* DosRST two-component regulatory system signaling by targeting response regulator DNA binding and sensor kinase heme

Huiqing Zheng[*], Bilal Aleiwi[†], Edmund Ellsworth[†], and Robert B. Abramovitch[*‡]

[1]Department of Microbiology and Molecular Genetics, [2]Department of Pharmacology and Toxicology, Michigan State University, East Lansing, Michigan, 48824

Supplemental Methods

Experimental procedures for urea formation

Formation of acyl chloride **2**. To a stirred solution of isoxazole acid **1** (1 eq.) in dry tetrahydrofuran (THF, 0.4 M) under N_2 atmosphere was added oxalyl chloride (1.5 eq.) dropwise over 5-10 min followed by dimethylformamide (DMF) (cat.) and the reaction mixture was continued to stir at room temperature. Upon completion, the reaction mixture was concentrated into a residue in *vacuo* and the residue was dissolved in THF and concentrated again to ensure the removal of excess oxalyl chloride. The crude acyl chloride **2** was used directly in the next step without further purification.

Formation of acyl azide and rearrangement into isocyanate **3**.

The crude acyl chloride **2** was dissolved in THF (0.4 M) and stirred at room temperature under N_2 atmosphere. Trimethylsilyl (TMS) azide (2 eq.) was added dropwise over 5 min and stirring was continued. Upon completion of the reaction, the mixture was diluted with ethyl acetate (0.4 M) and quenched with H_2O (0.4 M). The two layers were separated, and the organic layer was dried over anhydrous Na_2SO_4 and filtered. The ethyl acetate solvent was swapped into toluene (0.1 M) by the addition of toluene followed by removal of the ethyl acetate in *vacuo*. Care was taken not to concentrate the toluene. The toluene acyl azide solution was heated at reflux conditions under N_2 atmosphere for 4 h to give the desired isocyanate **3** which was used as a solution in toluene in the next step.

Formation of urea **4**. The crude isocyanate solution in toluene was mixed with different amines (1.5 eq.) and stirred at room temperature overnight. Isolation of the ureas was done by diluting the reaction mixture with hexanes, stirring for few hours and filtration of the formed precipitate. The solid material was washed with hexanes and dried under high vacuum. The urea products usually do not require further purifications. All products were analyzed by ^{1}H NMR and high-resolution mass spectrometry (HRMS).

Synthesis of ***MSU-41422*** (amide) from acyl chloride **2**. Acyl chloride **2** (1 eq.) was dissolved in dichloromethane (DCM, 0.2 M) and 4-chloroaniline (1.2 eq.) was added. The reaction mixture was stirred at room temperature overnight. The reaction mixture was concentrated in *vacuo* and the residue was purified by flash column chromatography.

Synthesis of ***MSU-39449***. A slurry of 4-chlorophenyl acetic acid (0.10 g, 0.60 mmoles) in 2.0 mL of DCM was treated with oxalyl chloride (0.12 mL, 0.9 mmoles) and 1 drop of DMF. The mixture (with gas evolution) gradually became homogeneous and was stirred for 30 min. The mixture was concentrated in *vacuo*, diluted with 5 mL of DCM and again concentrated in vacuo, the process repeated three times. The resulting residue was again dissolved in DCM (2 mL) and treated with 5-aminoisoxazole (0.030 g., 0.36 mmoles), followed by pyridine (0.48 mL, 0.6 mmoles). The mixture was then allowed to stir overnight. The mixture was then quenched with 1.0 N HCl and extracted with DCM. The organic layers were combined, washed with saturated $KHCO_3$, dried with Na_2SO_4 and concentrated in *vacuo*. Medium pressure liquid chromatography (SiO_2, 100% DCM to 3% methanol / DCM) to provide a solid (0.023 g).

^{1}H NMR and HRMS data:

MSU# 39444. ^{1}H NMR (500 MHz, DMSO-d_6) δ 10.54 (s, 2H), 8.44 (d, J = 1.9 Hz, 2H), 6.11 (d, J = 2.0 Hz, 2H). HRMS (ESI) m/z calculated for $C_7H_6N_4O_3$ [M+H], 195.0513 found 195.0518.

MSU# 39449. ^{1}H NMR (500 MHz, DMSO-d_6) δ 11.91 (s, 1H), 8.41 (s, 1H), 7.39 (d, J = 2.0 Hz, 2H), 7.35 (d, J = 2.0 Hz, 2H), 6.19 (s, 1H), 3.73 (s, 2H). HRMS (ESI) m/z calculated for $C_{11}H_{10}ClN_2O_2$ [M-H], 235.0269; found 235.1989.

MSU# 39445. ^{1}H NMR (500 MHz, DMSO-d_6) δ 10.41 (s, 1H), 9.14 (s, 1H), 8.40 (d, J = 2.0 Hz, 1H), 7.82 – 7.58 (m, 1H), 7.31 (dd, J = 4.9, 1.8 Hz, 2H), 7.07 (dt, J = 6.4, 2.3 Hz, 1H), 6.06 (d, J = 1.9 Hz, 1H). HRMS (ESI) m/z calculated for $C_{10}H_9ClN_3O_2$ [M+H], 238.0378; found 238.0365.

MSU# 39452. ^{1}H NMR (500 MHz, DMSO-d_6) δ 10.50 (s, 1H), 9.23 (s, 1H), 8.51 – 8.28 (m, 1H), 7.86 (d, *J* = 2.5 Hz, 1H), 7.64 – 7.43 (m, 1H), 7.37 (dd, *J* = 8.9, 2.5 Hz, 1H), 6.26 – 5.80 (m, 1H). HRMS (ESI) m/z calculated for $C_{10}H_8Cl_2N_3O_2$ [M+H], 271.9989; found 271.9969.

MSU# 39447. ^{1}H NMR (500 MHz, DMSO-d6) δ 8.83 (s, 1H), 8.43 – 8.29 (m, 1H), 7.36 (d, *J* = 8.4 Hz, 2H), 6.86 (d, *J* = 8.6 Hz, 2H), 6.00 (d, *J* = 1.9 Hz, 1H), 3.70 (s, 3H). HRMS (ESI) m/z calculated for $C_{11}H_{12}N_3O_3$ [M+H], 234.0874; found 234.0863.

MSU# 39451. ^{1}H NMR (500 MHz, DMSO-d6) δ 10.13 (s, 1H), 8.34 (d, *J* = 1.9 Hz, 1H), 7.56 – 7.41 (m, 2H), 7.41 – 7.22 (m, 2H), 6.04 (d, *J* = 2.0 Hz, 1H), 3.25 (s, 3H). HRMS (ESI) m/z calculated for $C_{11}H_{11}ClN_3O_2$ [M+H], 252.0535; found 252.0596.

MSU# 39453. ^{1}H NMR (500 MHz, DMSO-d6) δ 10.49 (s, 1H), 8.41 (d, *J* = 1.9 Hz, 1H), 7.84 (d, *J* = 8.7 Hz, 1H), 7.27 (dt, *J* = 2.3, 1.1 Hz, 1H), 7.18 (dt, *J* = 8.8, 1.6 Hz, 1H), 6.14 (d, *J* = 1.9 Hz, 1H), 4.13 (dd, *J* = 9.1, 8.2 Hz, 2H), 3.17 (t, *J* = 8.6 Hz, 2H). HRMS (ESI) m/z calculated for $C_{12}H_{11}ClN_3O_2$ [M+H], 264.0535; found 264.0552.

MSU# 39448. ^{1}H NMR (500 MHz, DMSO-d6) δ 10.55 (s, 1H), 9.25 (s, 1H), 8.64 – 8.24 (m, 2H), 7.98 (d, *J* = 8.6 Hz, 1H), 7.45 (d, *J* = 8.6 Hz, 1H), 6.08 (d, *J* = 18.1 Hz, 1H). HRMS (ESI) m/z calculated for $C_9H_8ClN_4O_2$ [M+H], 239.0331; found 239.0364.

MSU# 39450. ^{1}H NMR (500 MHz, DMSO-d6) δ 11.00 (s, 1H), 9.66 (s, 1H), 8.42 (d, *J* = 1.9 Hz, 1H), 8.34 (d, *J* = 2.6 Hz, 1H), 7.96 – 7.79 (m, 1H), 7.73 (d, *J* = 8.9 Hz, 1H), 6.10 (q, *J* = 2.7, 2.2 Hz, 2H). HRMS (ESI) m/z calculated for $C_9H_8ClN_4O_2$ [M+H], 239.0331; found 239.0356.

MSU# 39446. ^{1}H NMR (500 MHz, DMSO-d_6) δ 10.24 (s, 1H), 8.90 (s, 1H), 8.38 (d, *J* = 1.9 Hz, 1H), 7.54 – 7.37 (m, 2H), 7.26 – 7.02 (m, 2H), 6.03 (d, *J* = 2.0 Hz, 1H). HRMS (ESI) m/z calculated for $C_{10}H_9FN_3O_2$ [M+H], 222.0674; found 222.0675.

MSU# 41422. ^{1}H NMR (500 MHz, Chloroform-d) δ 8.41 (d, *J* = 1.8 Hz, 1H), 8.26 (s, 1H), 7.71 – 7.52 (m, 2H), 7.44 – 7.33 (m, 2H), 7.06 (d, *J* = 1.8 Hz, 1H). HRMS (ESI) m/z calculated for $C_{10}H_8ClN_2O_2$ [M+H], 223.0269; found 223.0265.

MSU# 41324. ^{1}H NMR (500 MHz, DMSO-d6) δ 9.91 (s, 1H), 9.50 (s, 1H), 8.31 (d, *J* = 2.6 Hz, 1H), 7.85 (dd, *J* = 9.0, 2.7 Hz, 1H), 7.67 (d, *J* = 8.9 Hz, 1H), 7.39 – 7.30 (m, 2H). HRMS (ESI) m/z calculated for $C_{12}H_{10}Cl_2N_3O$ [M+H], 282.0196; found 282.0182.

MSU# 41425. ^{1}H NMR (500 MHz, DMSO-d_6) δ 8.83 (s, 1H), 7.53 – 7.39 (m, 2H), 7.39 – 7.16 (m, 2H). HRMS (ESI) m/z calculated for $C_{13}H_{11}Cl_2N_2O$ [M+H], 281.0243; found 281.0258.

MSU# 41443. ^{1}H NMR (500 MHz, DMSO-d_6) δ 10.36 (d, *J* = 28.4 Hz, 1H), 9.13 (d, *J* = 45.7 Hz, 1H), 8.40 (d, *J* = 1.9 Hz, 1H), 7.70 – 7.59 (m, 5H), 7.59 – 7.49 (m, 3H), 7.43 (t, *J* = 7.7 Hz, 3H), 7.32 (t, *J* = 7.4 Hz, 1H), 6.06 (d, *J* = 1.9 Hz, 1H). HRMS (ESI) m/z calculated for $C_{16}H_{14}N_3O_2$ [M+H], 280.1081; found 280.1083.

MSU# 41442. ^{1}H NMR (500 MHz, DMSO-d6) δ 10.15 (s, 1H), 8.77 (s, 1H), 8.38 (d, *J* = 1.9 Hz, 1H), 7.44 – 7.27 (m, 4H), 6.03 (d, *J* = 2.0 Hz, 1H), 1.25 (s, 9H). HRMS (ESI) m/z calculated for $C_{14}H_{18}N_3O_2$ [M+H], 260.1394; found 260.1406.

MSU# 33189. ^{1}H NMR (500 MHz, DMSO-d_6) δ 10.20 (s, 1H), 8.85 (s, 1H), 8.39 (d, *J* = 1.9 Hz, 1H), 7.54 – 7.37 (m, 2H), 7.35 – 7.21 (m, 2H), 7.02 (t, *J* = 7.4 Hz, 1H), 6.04 (d, *J* = 1.9 Hz, 1H). HRMS (ESI) m/z calculated for $C_{10}H_{10}N_3O_2$ [M+H], 204.0768; found 204.0777.

MSU# 33231. ^{1}H NMR (500 MHz, DMSO-d6) δ 10.29 (s, 1H), 9.01 (s, 1H), 8.39 (d, *J* = 1.9 Hz, 1H), 7.56 – 7.41 (m, 2H), 7.41 – 7.27 (m, 2H), 6.05 (d, *J* = 1.9 Hz, 1H). HRMS (ESI) m/z calculated for $C_{10}H_9ClN_3O_2$ [M+H], 238.0378; found 238.0391.

MSU# 41462. ^{1}H NMR (500 MHz, DMSO-d_6) δ 10.18 (s, 1H), 8.31 (d, *J* = 2.0 Hz, 1H), 7.43 – 7.07 (m, 3H), 6.92 (s, 1H), 5.94 (d, *J* = 1.9 Hz, 1H), 4.30 (d, *J* = 6.0 Hz, 2H). HRMS (ESI) m/z calculated for $C_{11}H_{12}N_3O_2$ [M+H], 218.0924 found 218.0956.

MSU# 41463. ^{1}H NMR (500 MHz, DMSO-d_6) δ 10.39 (s, 1H), 9.29 (s, 1H), 8.41 (d, *J* = 1.9 Hz, 1H), 7.67 (d, *J* = 1.0 Hz, 4H), 6.08 (d, *J* = 1.9 Hz, 1H). HRMS (ESI) m/z calculated for $C_{11}H_9F_3N_3O_2$ [M+H], 272.0642; found 272.0653.

MSU# 41464. ^{1}H NMR (500 MHz, DMSO-d_6) δ 10.29 (s, 1H), 9.01 (s, 1H), 8.39 (d, *J* = 1.9 Hz, 2H), 7.50 – 7.45 (m, 1H), 7.45 – 7.40 (m, 1H), 6.05 (s, 1H). HRMS (ESI) m/z calculated for $C_{10}H_9BrN_3O_2$ [M+H], 281.9873; found 281.9876.

MSU# 41465. ^{1}H NMR (500 MHz, DMSO-d_6) δ 10.38 (s, 1H), 9.27 (s, 1H), 8.41 (d, *J* = 2.0 Hz, 1H), 8.00 – 7.79 (m, 2H), 7.66 – 7.48 (m, 2H), 6.08 (d, *J* = 1.9 Hz, 1H), 3.81 (s, 3H). HRMS (ESI) m/z calculated for $C_{12}H_{12}N_3O_4$ [M+H], 262.0823; found 262.0827.

MSU# 41545. ^{1}H NMR (500 MHz, DMSO-d_6) δ 10.17 (s, 1H), 8.71 (s, 1H), 8.37 (d, *J* = 1.9 Hz, 1H), 7.57 – 7.14 (m, 5H), 7.11 – 6.69 (m, 2H), 6.02 (d, *J* = 1.9 Hz, 1H), 5.06 (s, 2H).HRMS (ESI) m/z calculated for $C_{17}H_{16}N_3O_3$ [M+H], 310.1187; found 310.1178.

MSU# 41546. ^{1}H NMR (500 MHz, DMSO-d_6) δ 9.69 (s, 1H), 8.30 (d, *J* = 1.9 Hz, 1H), 6.42 (d, *J* = 7.2 Hz, 1H), 5.91 (d, *J* = 1.9 Hz, 1H), 3.92 (h, *J* = 6.7 Hz, 1H), 1.83 (dq, *J* = 12.8, 6.6, 6.0 Hz, 3H), 1.73 – 1.46 (m, 5H), 1.46 – 1.13 (m, 3H). HRMS (ESI) m/z calculated for $C_9H_{14}N_3O_2$ [M+H], 196.1081; found 196.1144.

MSU# 42002. ^{1}H NMR (500 MHz, DMSO-d_6) δ 9.80 (s, 1H), 8.30 (d, *J* = 1.9 Hz, 1H), 6.34 (d, *J* = 7.8 Hz, 1H), 5.90 (d, *J* = 1.9 Hz, 1H), 3.58 – 3.39 (m, 1H), 1.77 (dt, *J* = 11.1, 3.7 Hz, 1H), 1.64 (dt, *J* = 12.9, 4.1 Hz, 1H), 1.52 (dd, *J* = 10.4, 6.3 Hz, 1H), 1.37 – 0.93 (m, 3H). HRMS (ESI) m/z calculated for $C_{10}H_{16}N_3O_2$ [M+H], 210.1238; found 210.1282.

MSU# 42004. ^{1}H NMR (500 MHz, DMSO-d_6) δ 10.07 (s, 2H), 8.31 (d, *J* = 2.0 Hz, 1H), 7.37 – 7.06 (m, 5H), 6.40 (s, 1H), 5.93 (d, *J* = 1.8 Hz, 1H), 3.31 (t, *J* = 7.2 Hz, 2H), 2.74 (t, *J* = 7.2 Hz, 2H). HRMS (ESI) m/z calculated for $C_{12}H_{14}N_3O_2$ [M+H], 232.1081; found 232.1105.

MSU# 42003. ^{1}H NMR (500 MHz, DMSO-d_6) δ 10.36 (s, 1H), 9.06 (s, 1H), 8.40 (d, *J* = 1.9 Hz, 1H), 7.83 (t, *J* = 2.0 Hz, 1H), 7.46 – 7.03 (m, 3H), 6.07 (d, *J* = 2.0 Hz, 1H). HRMS (ESI) m/z calculated for $C_{10}H_9BrN_3O_2$ [M+H], 281.9873; found 281.9915.

MSU# 41542. ^{1}H NMR (500 MHz, DMSO-d_6) δ 10.20 – 9.49 (m, 1H), 8.30 (d, *J* = 1.9 Hz, 1H), 6.44 (t, *J* = 5.9 Hz, 1H), 5.91 (d, *J* = 1.9 Hz, 1H), 2.93 (t, *J* = 6.3 Hz, 2H), 1.68 (dh, *J* = 13.3, 6.7

Hz, 1H), 0.85 (d, *J* = 6.7 Hz, 6H). HRMS (ESI) m/z calculated for $C_8H_{14}N_3O_2$ [M+Na], 206.0899; found 206.0926.

Supplementary Dataset 1. Differential gene expression data of WT Mtb treated with inhibitors

Supplementary Dataset 2. Differential gene expression data of the DosR mutant treated with the inhibitors.

Supplementary Dataset 3. Complete gene expression tables for transcriptional profiling experiments.

Supplemental Table 1 and Figures 1-9

Compound	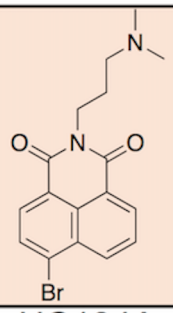	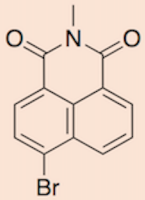	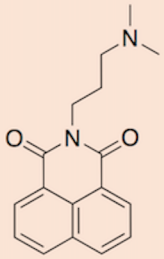
ID#	HC104A	HC104G	HC104B
MW (g/mole)	361.2	290.1	282.3
EC_{50} (μM)	9.8	43.8	>200
Ligand Efficiency	0.34	0.36	0.26
CLogP (cLogD at pH 7.4)	3.0 (0.55)	2.3 (2.4)	2.9 (-0.24)
Druglikeness	4.4	0.55	6.2

Supplemental Table 1. Structure and properties of HC104 series. Catalog structure activity relationship study performed for HC104 analogs with different R-groups. The reporter strain CDC1551 (hspX'::GFP) was treated across doses of each analog from 200 μM to 0.328 μM. The EC50 values of fluorescence inhibition calculated for each analog to determine their potency. The other chemical properties of the analogs are also included.

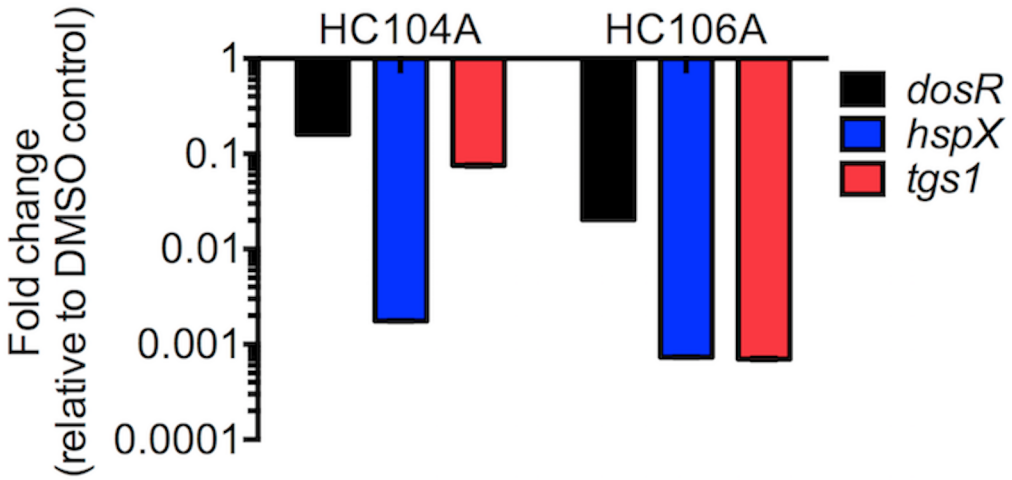

Supplemental Figure 1. Inhibition of the DosR regulon by HC104 and HC106A during hypoxia. Mtb cells were treated with 40 μM compounds for 6 d, and total bacterial RNA was isolated. The DosR regulated genes, dosR, hspX, and tgs1 were quantified in qRT-PCR. The error bars represent the standard derivation of three replicates. The experiment was repeated at least twice with similar results.

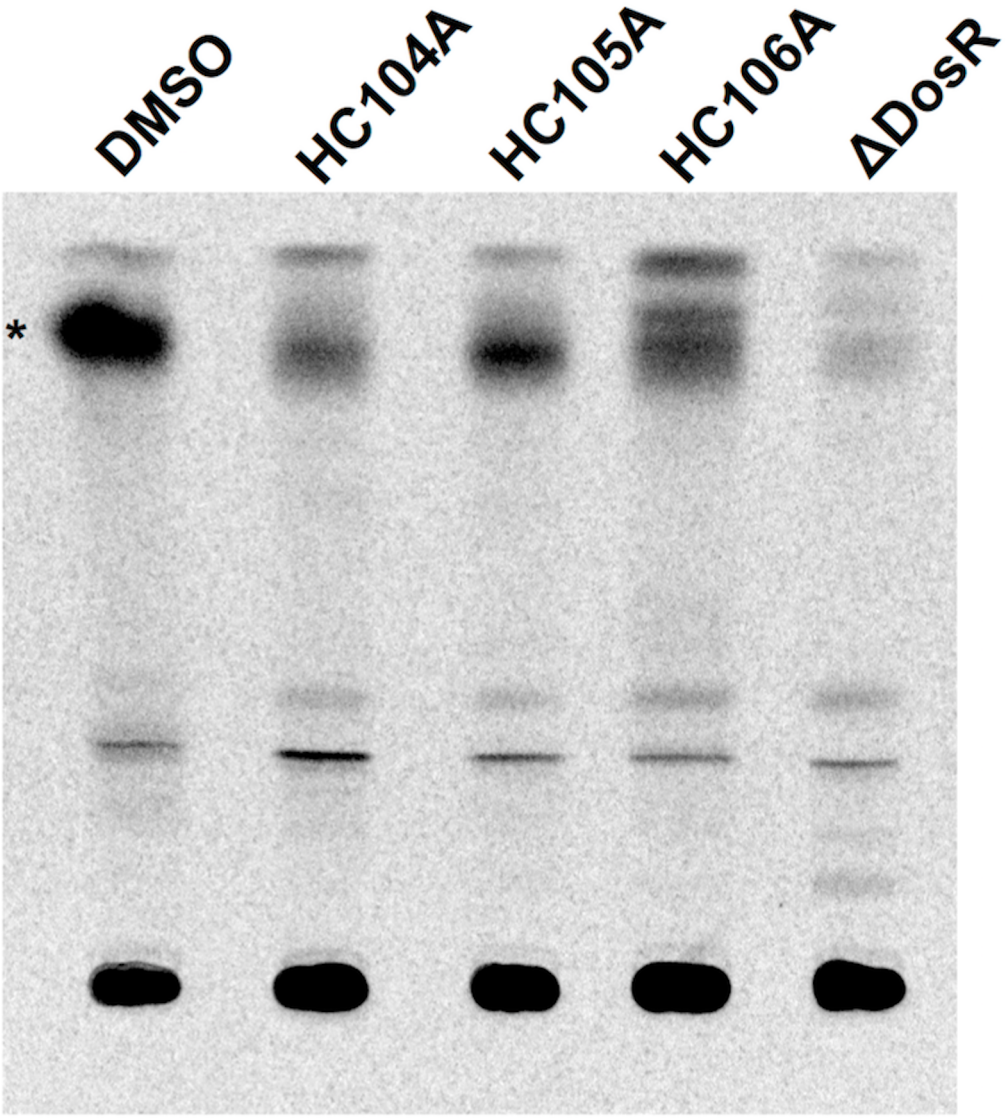

Supplemental Figure 2. TLC of TAG reduction in Mtb treated with HC104A and HC106A. Mtb cells were treated with 40 μM of the compounds and labeled with [1,2-14C] sodium acetate in T25 vented tissue culture flasks for 6 d. Total lipid was isolated and analyzed BY TLC. The experiment was repeated twice with similar results.

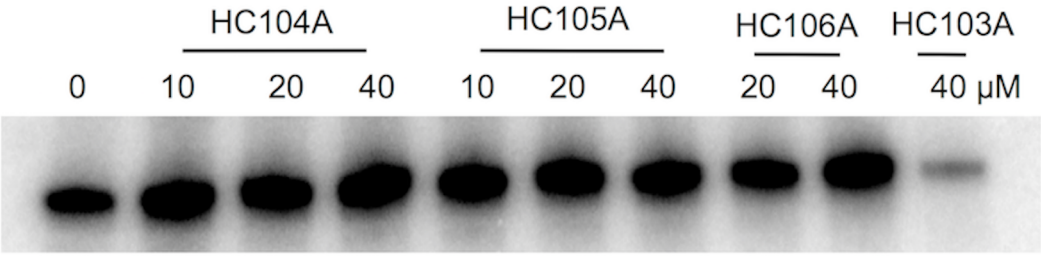

Supplemental Figure 3. Autoradiograph examining the impact of HC104A and HC106A on DosS autophosphorylation. DosS protein was treated with 10 μM, 20 μM or 40 μM of the compounds, with DMSO and HC103A as positive and negative controls, respectively. The results show that HC104A and HC106A have no effect on DosS autophosphorylation.

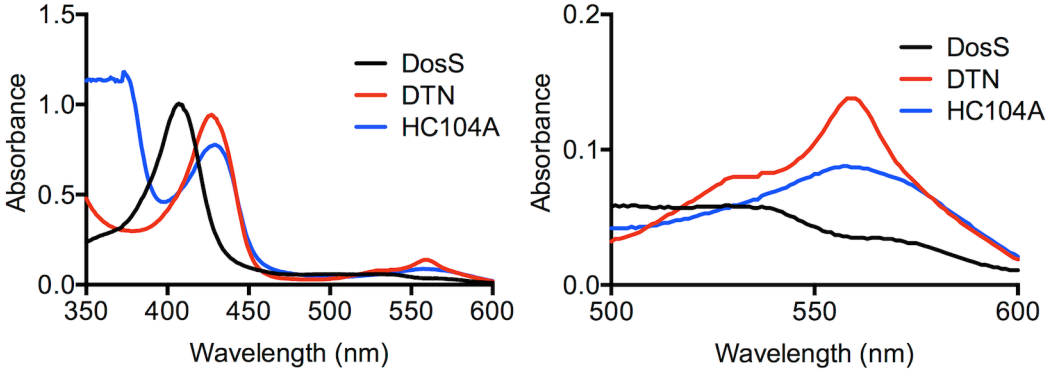

Supplemental Figure 4. Investigation of interaction between HC104A and DosS. WT DosS treated with 400 μM HC104A shows no impact on shifting of the Soret peak in the UV-visible spectroscopy assay. The experiment was repeated at least twice with similar results.

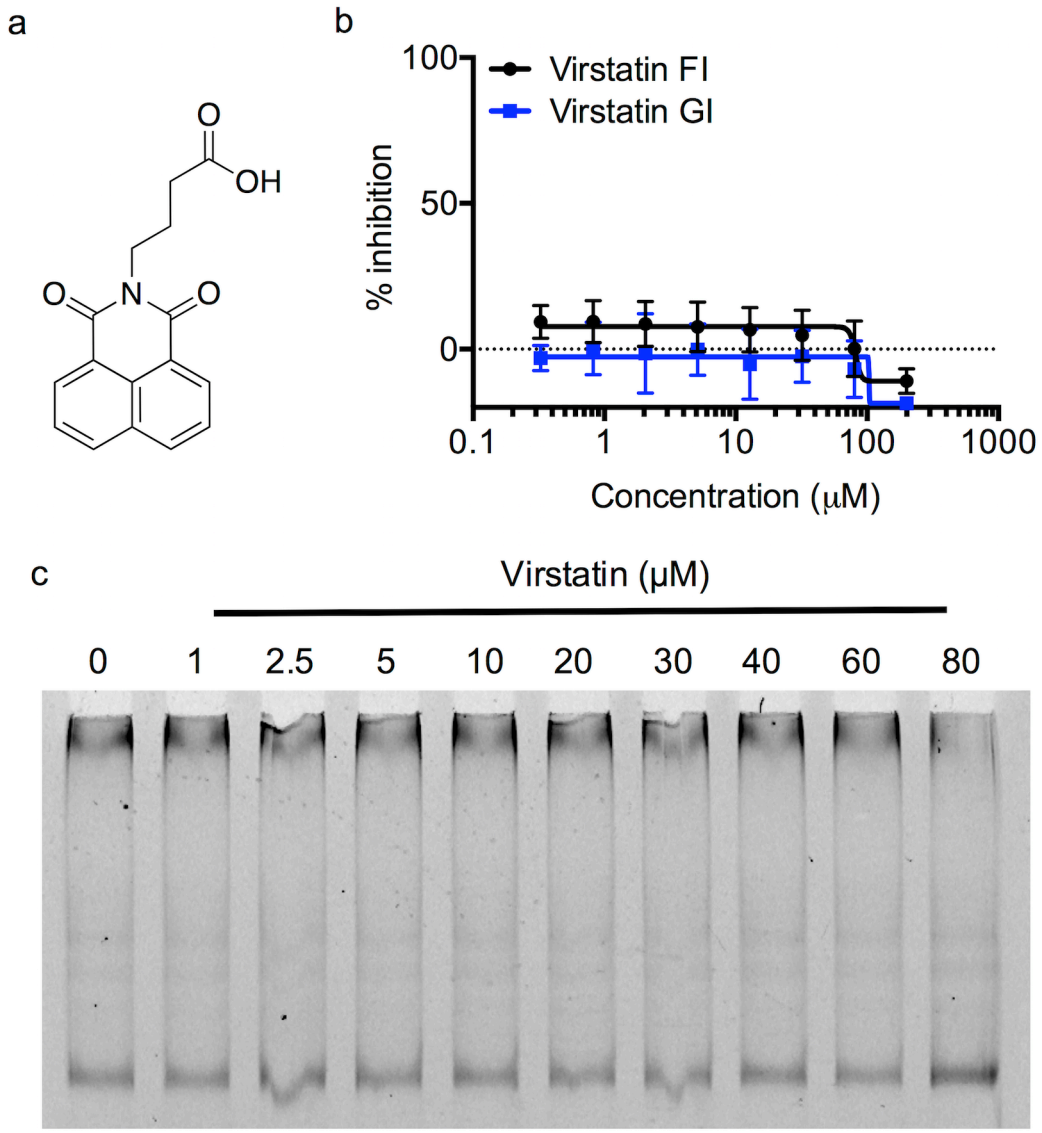

Supplemental Figure 5. The impact of virstatin on DosR DNA-binding and DosRST signaling in Mtb. (a) Chemical structure of virstatin. (b) Dose-response curve of virstatin shows no effect on inhibition of Mtb DosR-driven GFP fluorescence. (c) DosR protein at 2 μM was treated with 9 point dose response of virstatin from 1 μM to 80 μM. The reactions were analyzed on native PAGE gel. The experiment was repeated at least twice with similar results.

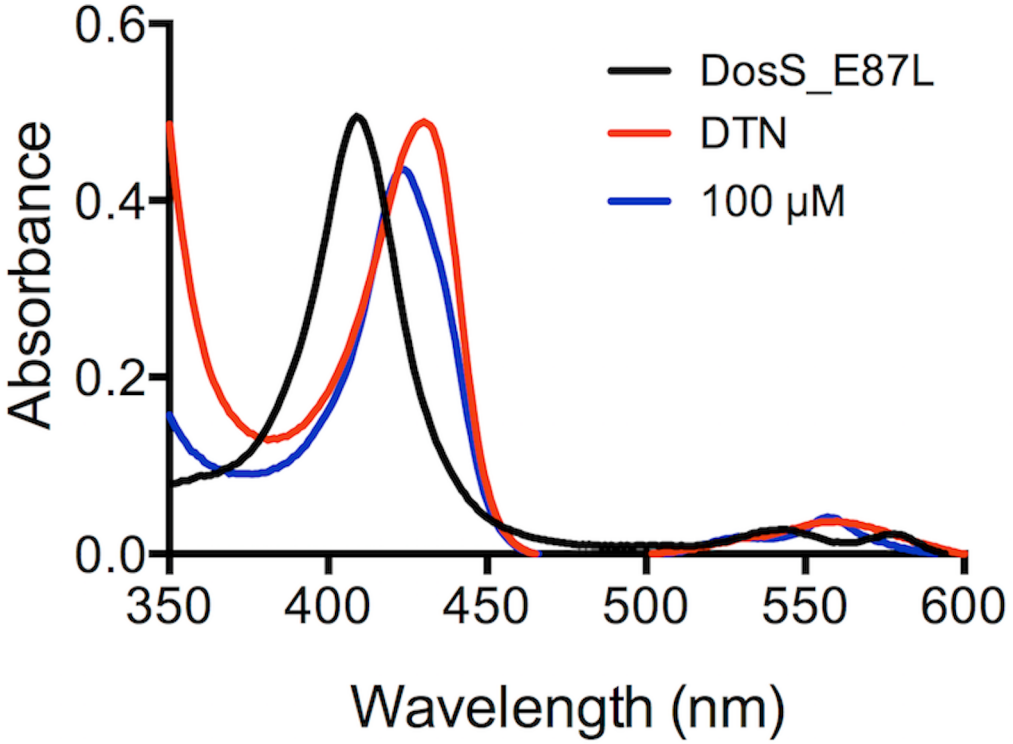

Supplemental Figure 6. Investigating the interaction between HC106A and DosS heme. DosS E87L protein was treated with 100 μM HC106A after being reduced with DTN. The UV-visible spectra were recorded after each treatment, and showed no change on the overall spectrum compared to WT protein. The experiment was repeated at least twice with similar results.

A

HC103A (μM)

HC102A (μM)	50	20	8	3.2	1.28	0.51	0.21	0.08
50	0.14	0.28	0.43	0.34	0.38	0.44	0.5	0.49
20	0.19	0.39	0.32	0.33	0.41	0.58	0.75	0.82
8	0.21	0.45	0.38	0.47	0.62	0.91	1.13	1.33
3.2	0.3	0.55	0.61	0.71	0.99	1.18	1.49	1.89
1.28	0.44	0.72	0.9	1.14	1.22	1.55	1.87	2.99
0.51	0.43	0.85	1.11	1.24	1.28	1.35	1.86	4.2
0.21	0.43	0.94	1.19	1.37	1.4	1.59	3.61	13.8
0.08	0.43	0.94	1.2	1.32	1.27	1.18	1.51	5.84

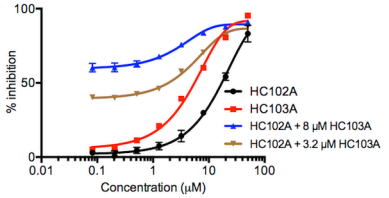

HC104A (μM)

HC102A (μM)	50	20	8	3.2	1.28	0.51	0.21	0.08
50	0.33	0.53	0.85	0.77	0.76	0.77	0.75	0.74
20	0.33	0.73	1.06	1.12	1.19	1.19	1.13	1.04
8	0.31	0.89	1.36	1.64	1.76	1.75	1.69	1.57
3.2	0.28	1.06	1.58	1.91	2.13	2.06	2.18	2.32
1.28	0.28	1.11	1.65	2.05	2.3	2.67	3.05	7.27
0.51	0.27	1.11	1.66	1.95	2.27	2.6	3.81	46.9
0.21	0.29	1.12	1.68	2.06	2.26	3.21	5.22	5.7
0.08	0.27	1.09	1.61	1.9	2.17	2.28	3.1	9.43

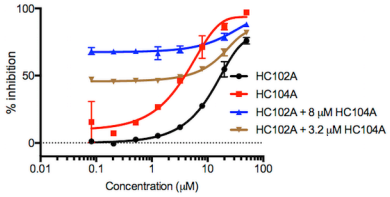

HC106A (μM)

HC102A (μM)	50	20	8	3.2	1.28	0.51	0.21	0.08
50	0.82	0.37	0.33	0.31	0.33	0.39	0.44	0.5
20	0.85	0.4	0.43	0.46	0.49	0.58	0.63	0.7
8	0.64	0.42	0.8	0.9	0.81	0.82	0.99	1.05
3.2	0.71	0.42	1.36	1.29	1.18	1.62	1.12	1.27
1.28	0.72	0.42	1.64	1.69	1.4	1.3	1.3	1.47
0.51	0.72	0.44	1.74	1.59	1.47	1.21	1.24	1.32
0.21	0.7	0.41	1.78	1.87	1.52	1.35	1.49	1.72
0.08	0.71	0.43	1.66	1.67	1.37	1.25	1.14	0.91

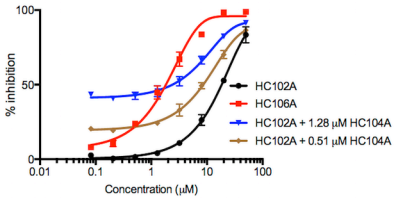

HC104A (μM)

HC103A (μM)	50	20	8	3.2	1.28	0.51	0.21	0.08
50	0.67	0.29	0.35	0.44	0.48	0.64	0.56	0.55
20	0.52	0.5	0.79	0.96	1.11	1.3	1.17	1.22
8	0.45	0.76	1.03	1.22	1.38	1.56	1.54	1.47
3.2	0.42	1.01	1.23	1.35	1.49	1.87	1.92	1.72
1.28	0.39	1.07	1.34	1.42	1.52	1.76	1.87	1.91
0.51	0.4	1.13	1.43	1.47	1.5	1.53	0.95	2.02
0.21	0.39	1.16	1.43	0.94	1.41	1.41	1.78	3.2
0.08	0.16	1.18	1.44	1.47	1.44	1.24	1.26	3.37

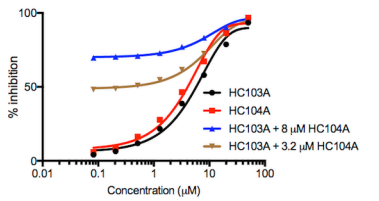

HC106A (μM)

HC103A (μM)	50	20	8	3.2	1.28	0.51	0.21	0.08
50	1.23	0.54	0.3	0.22	0.2	0.27	0.35	0.51
20	1.04	0.44	0.2	0.25	0.39	0.74	0.81	1.03
8	0.96	0.43	0.3	0.72	0.65	0.79	1	1.19
3.2	0.78	0.41	0.6	0.89	0.96	1	1.13	1.24
1.28	0.87	0.44	1.1	1.56	1.38	1.37	1.29	1.3
0.51	0.82	0.48	1.5	1.95	1.64	1.61	1.59	1.44
0.21	0.89	0.48	1.9	2.16	1.93	1.73	1.99	2.5
0.08	0.82	0.46	2.2	2.08	2.29	1.79	2.1	2.74

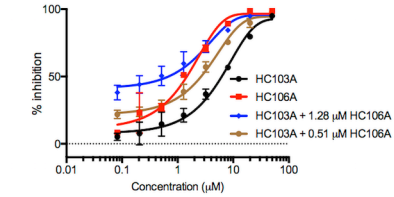

HC106A (μM)

HC104A (μM)	50	20	8	3.2	1.28	0.51	0.21	0.08
50	1.79	1.05	0.65	0.51	0.45	0.44	0.86	0.55
20	1.35	0.64	0.52	0.65	0.83	0.99	1.11	1.16
8	1.05	0.53	0.78	0.97	1.11	1.38	1.52	1.55
3.2	0.84	0.48	0.96	1.11	1.22	1.45	1.58	1.62
1.28	0.77	0.51	1.29	1.68	1.42	1.73	1.67	1.64
0.51	0.88	0.52	1.44	1.45	1.47	1.64	1.68	1.46
0.21	0.8	0.4	1.72	1.62	0.94	1.3	1.76	1.51
0.08	0.79	0.44	1.69	1.59	1.43	1.5	1.46	1.35

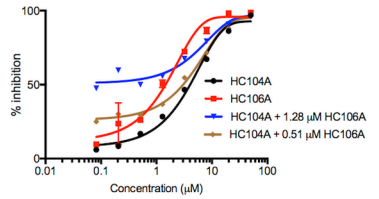

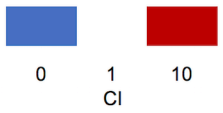

Supplemental Figure 7. Checkerboard assays examining paired interactions of DosRST inhibitors. CDC1551 (hspX'::GFP) was treated with different combination of two compounds from 50 μM to 0.08 μM. GFP fluorescence was measured and used to calculate percentage inhibition. The data were analyzed in the CompuSyn software to determine the combination index (CI) for the panel of each drug combination, including (a) artemisinin and HC104A; (b) HC102A and HC103A; (c) HC102A and HC104A; (d) HC102A and HC106A; (e) HC103A and HC104A; (f) HC103A and HC106A; (g) HC104A and HC106A. Selected dose response curves are presented to illustrate synergistic interactions. The experiment was repeated twice with similar results.

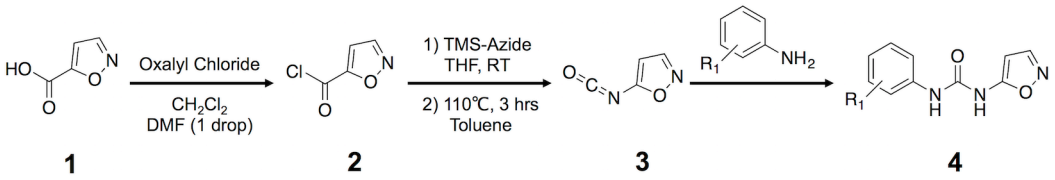

Supplemental Figure 8. Synthetic scheme for the HC106 analogs.

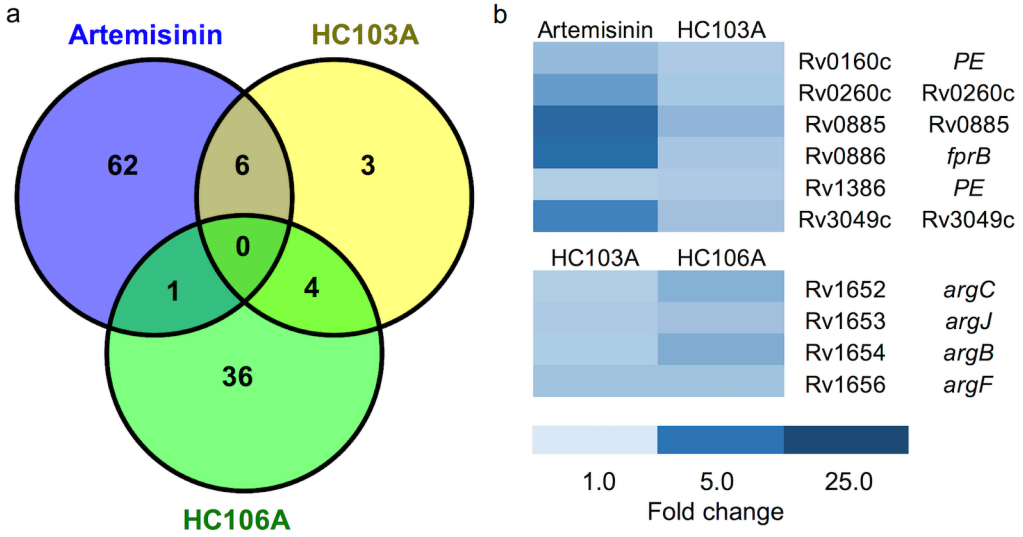

Supplemental Figure 9. Comparison between artemisinin, HC103 and HC106 for interactions. (a) Venn diagram for the downregulated genes (>2-fold; q< 0.05) of CDC1551 (ΔdosR) treated with artemisinin, HC103A, or HC106A. (b) Overlap exists between artemisinin and HC103A or HC103A and HC106A differentially expressed genes (downregulated >2X, q<0.05). The heatmaps represent the commonly downregulated genes between the two compounds.